Electron Energy-Loss Spectroscopy (EELS)

Rantanen Aleksi and Sonphasit Jasmin

Table of contents:

Introduction

- EELS or Electron Energy Loss Spectroscopy is a spectroscopic technique similar to Energy Dispersive Spectroscopy (EDS) that is used to detect elemental compositions of materials (and more!)
- The main difference between EDS and EELS is that EELS can detect **different allotropes of the same element**, for example if carbon is in the form of graphite or diamond
- The main principle of the technique is that the electron beam hits the sample and **inelastically scattered electrons** are separated by their energies using a magnetic field
- Electrons lose energies by a variety of mechanisms, so the created energy spectrum can be used to determine **a wide range of information**, such as bonding properties, valence electronic structure, and unoccupied states
- EELS can be mounted for example on a transmission electron microscope (TEM)

Equipment

- EELS can be mounted below the TEM column
- Electron beam is generated in the electron source
- The electrons scatter by different mechanisms, and for EELS the inelastically scattered primary beam electrons are used
- The inelastically scattered electrons with different energies are separated by a magnetic prism or omega type filter

https://wiki.aalto.fi/display/SSC/Electron+Energy+Loss+Spectroscopy

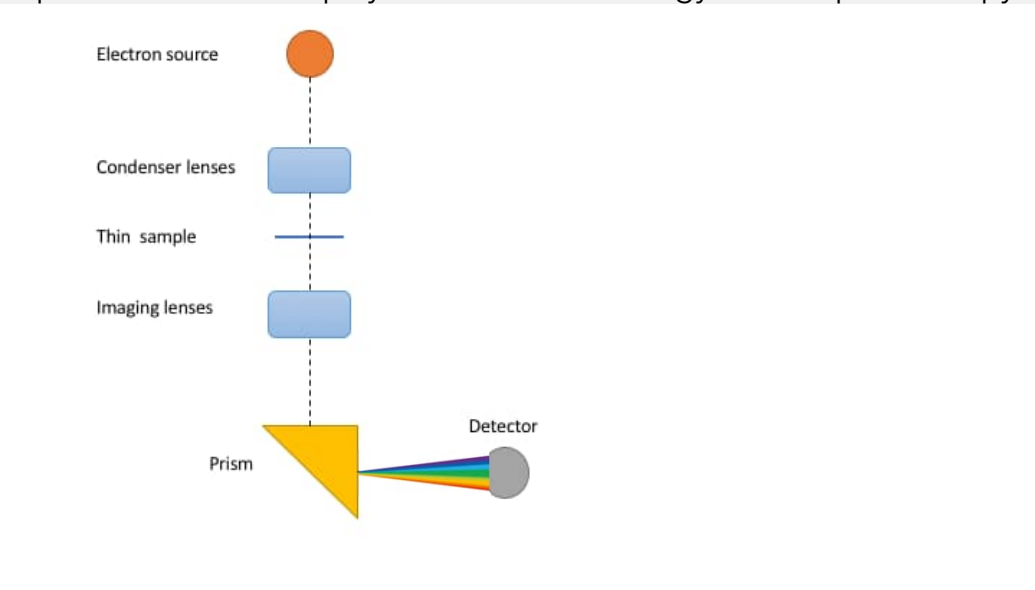

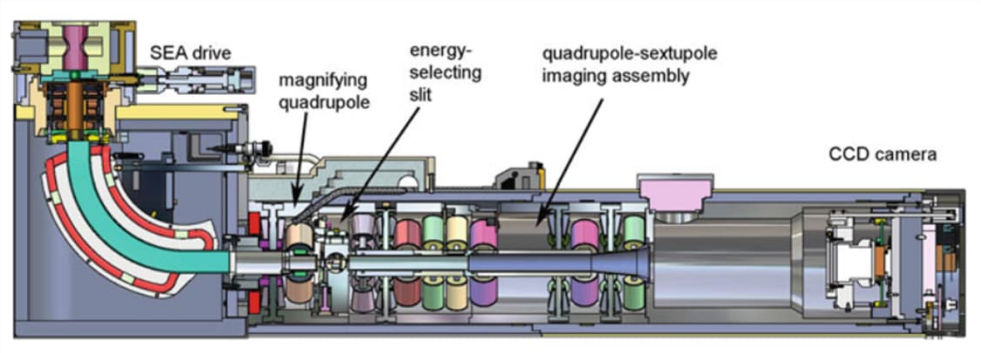

R.F. Egerton. Electron Energy-Loss Spectronscopy in the Electron Microscope

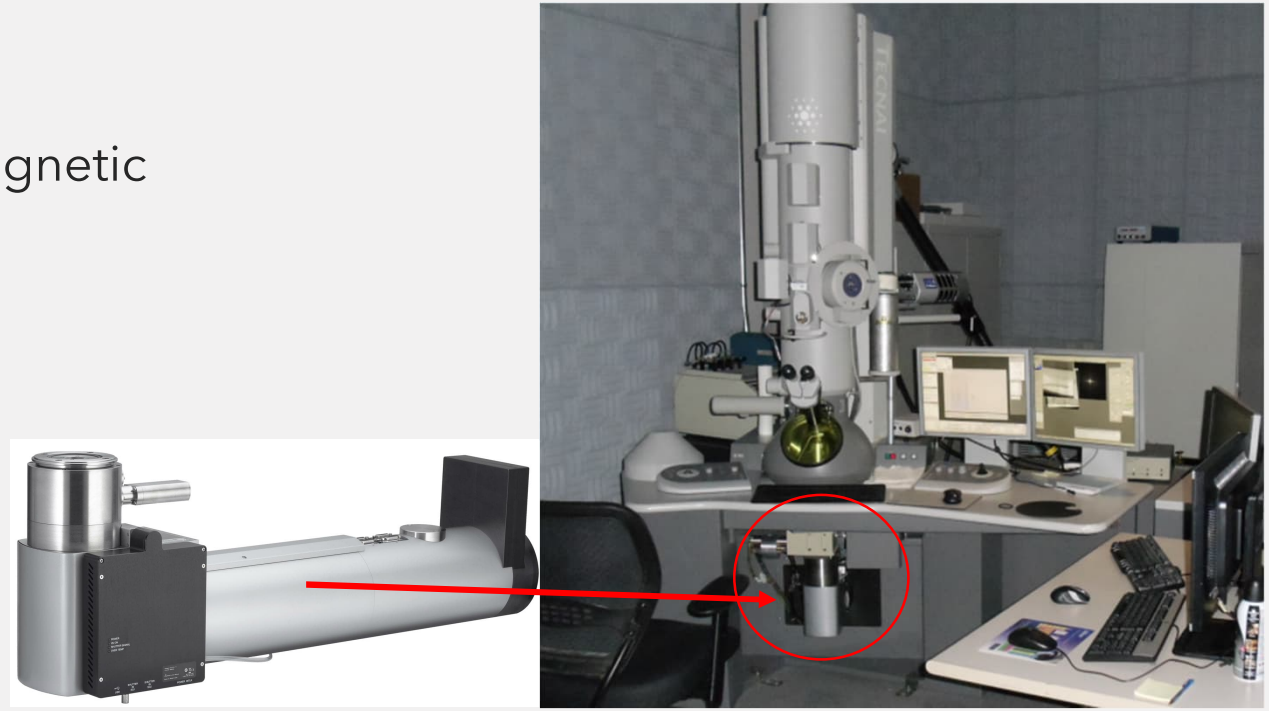

https://www.nanolabtechnologies.com/tem-stem-eels-eds/

Equipment

- EELS can be mounted below the TEM column
- Electron beam is generated in the electron source
- The electrons scatter by different mechanisms, and for EELS the inelastically scattered primary beam electrons are used
- The inelastically scattered electrons with different energies are separated by a magnetic prism or omega type filter
- Different energies are selected using energy selecting slit
- The spectrum is created as the electrons hit the detector (CCD camera)

https://wiki.aalto.fi/display/SSC/Electron+Energy+Loss+Spectroscopy

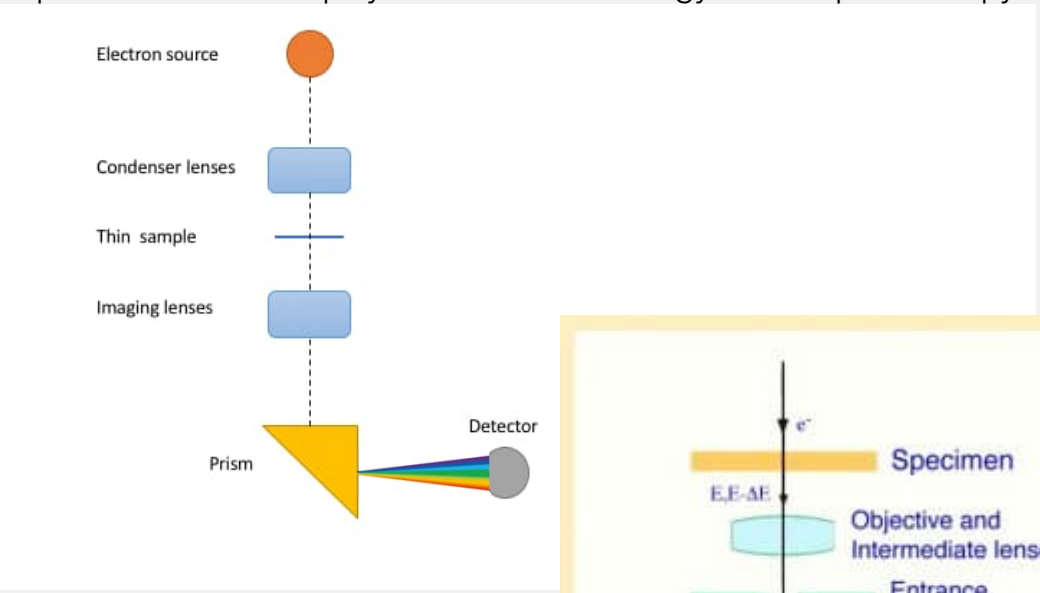

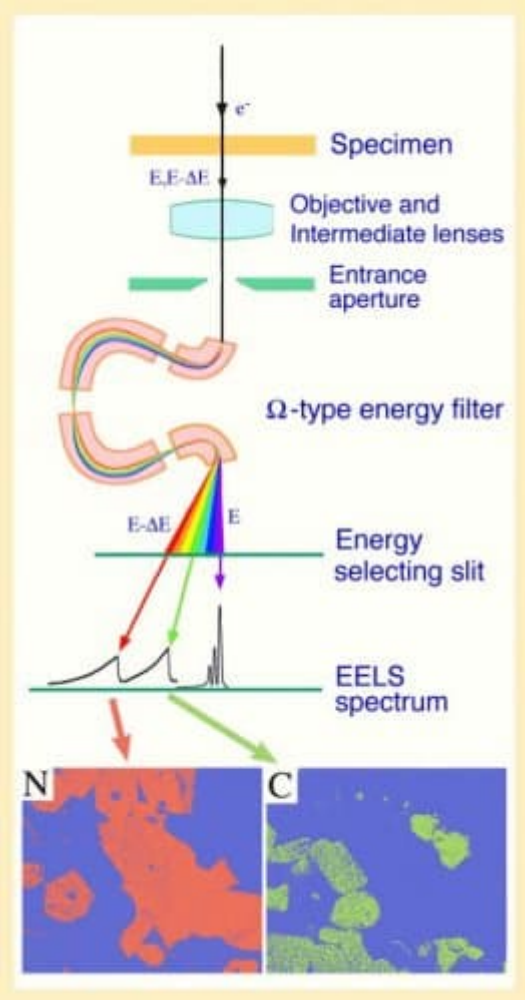

http://www2.tagen.tohoku.ac.jp/lab/terauchi/html/research/instruments/jem2010fef.html

Principle of the Technique

- Inelastic scattering occurs when the interaction with the sample causes loss of energy in the primary electron
- Inelastic scattering creates **a range of useful signals** that can be exploited to characterize the material

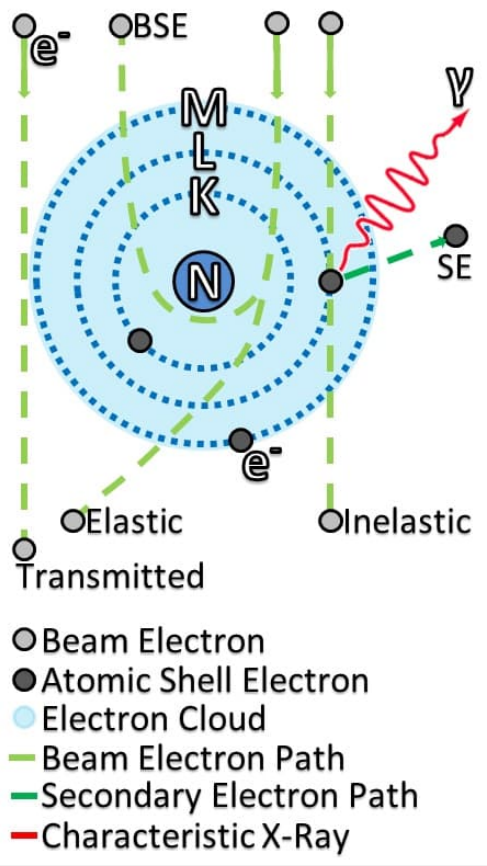

Principle of the Technique

- Inelastic scattering occurs when the interaction with the sample causes loss of energy in the primary electron
- Inelastic scattering creates **a range of useful signals** that can be exploited to characterize the material
- These signals are separated in a spectrum of energies and these energies are separated in low loss (<50 eV) and high loss (>50 eV) ranges
- Low loss:
  - The **zero loss** peak is caused by elastic scattering (no energy loss) all other interactions are inelastic
  - **Plasmons** are resonances of the valence electrons
  - **Interband transitions** are single electron interactions

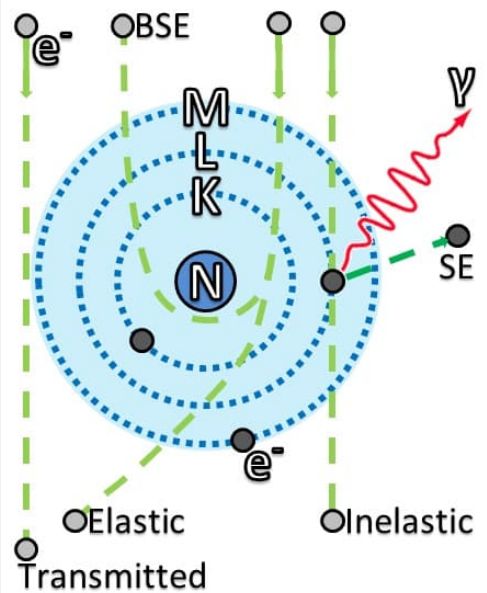

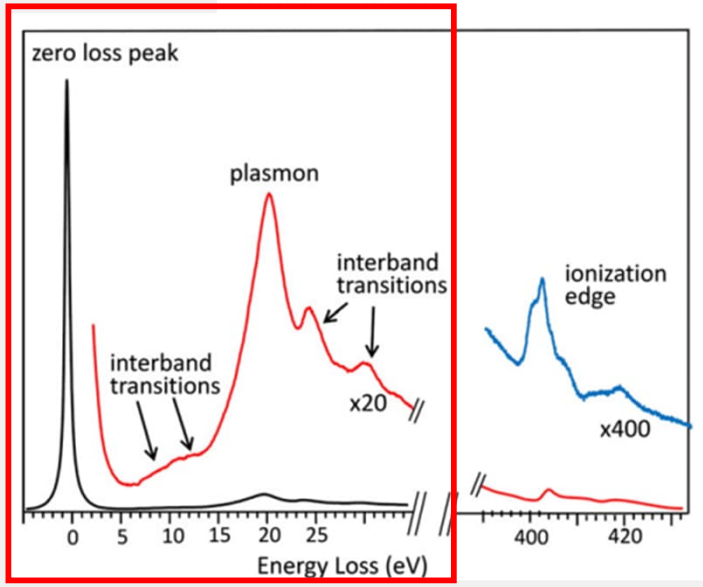

Principle of the Technique

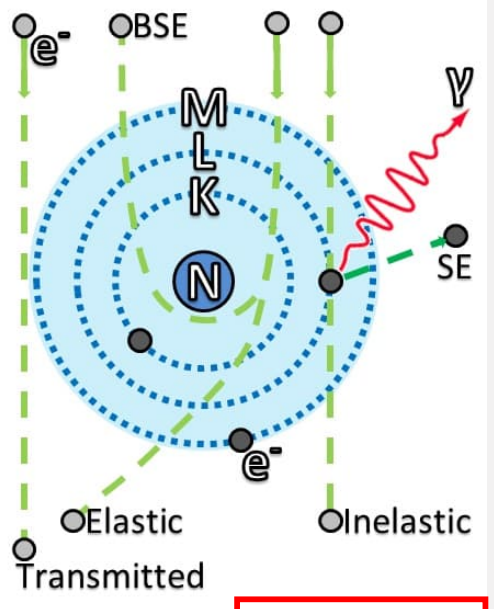

- Inelastic scattering occurs when the interaction with the sample causes loss of energy in the primary electron
- Inelastic scattering creates **a range of useful signals** that can be exploited to characterize the material
- These signals are separated in a spectrum of energies and these energies are separated in low loss (<50 eV) and high loss (>50 eV) ranges
- Low loss:
  - The **zero loss** peak is caused by elastic scattering (no energy loss) all other interactions are inelastic
  - **Plasmons** are resonances of the valence electrons
  - **Interband transitions** are single electron interactions
- High loss:
  - **Ionization edges** are created from interaction with inner shell electrons, causing excitation of the electron to a higher energy state and resulting in a characteristic elemental energy loss
  - **Energy loss near edge structure (ELNES)** and **extended energy loss fine structure (EXELFS)** are used for bonding and structure determination

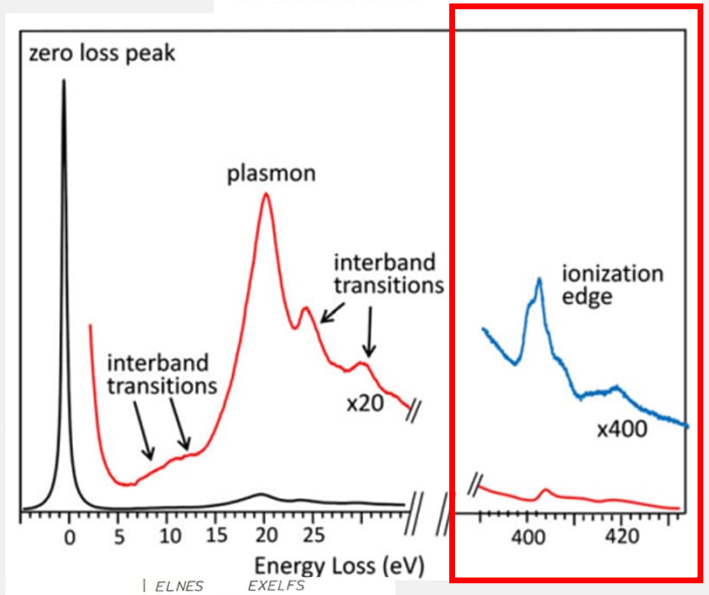

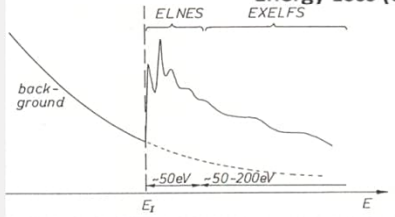

Chemistry

- Different elements create absorption edges at different energies, but the shapes are also determined by the bonding of the cations.
- The strong L-edge peaks are created by high density of vacant d-states

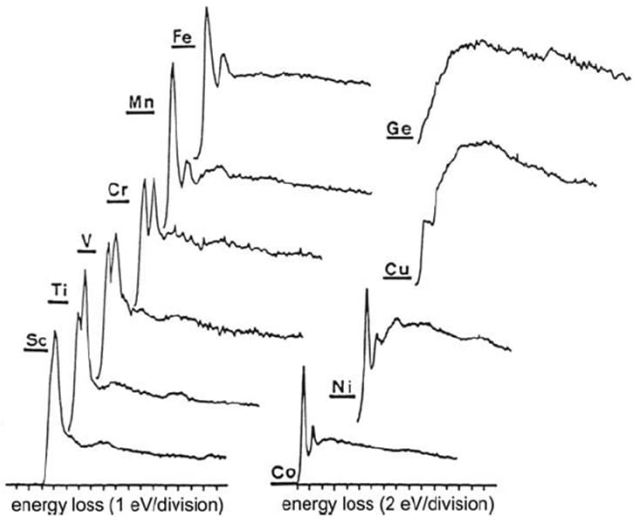

Fig. 3.45 *L*-edges of fourth-period elements measured using 120-keV electrons and a collection semi-angle of 5.7 mrad. From Zaluzec (1982), copyright Elsevier

Fig. 3.46 Cu L_{23} edges in metallic copper and in cupric oxide, measured using 75-keV electrons scattered up to $\beta = 2$ mrad. From Leapman et al. (1982), copyright American Physical Society. Available at http://link.aps.org/abstract/PRB/v26/p614

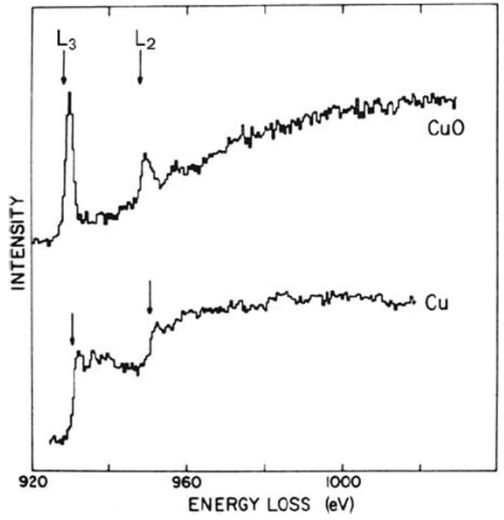

R.F. Egerton. Electron Energy-Loss Spectronscopy in the Electron Microscope

Chemistry

- Different elements create absorption edges at different energies, but the shapes are also determined by the bonding of the cations.
- The strong L-edge peaks are created by high density of vacant d-states
- In metallic Cu the d band is full and similar peaks are not seen

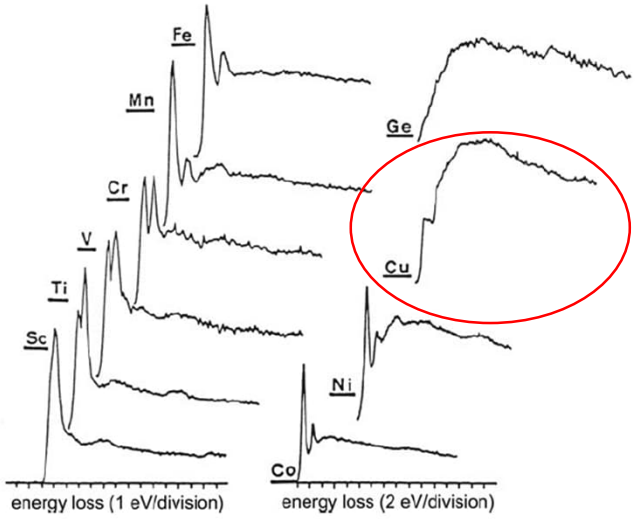

Fig. 3.45 *L*-edges of fourth-period elements measured using 120-keV electrons and a collection semi-angle of 5.7 mrad. From Zaluzec (1982), copyright Elsevier

Fig. 3.46 Cu L_{23} edges in metallic copper and in cupric oxide, measured using 75-keV electrons scattered up to $\beta = 2$ mrad. From Leapman et al. (1982), copyright American Physical Society. Available at http://link.aps.org/abstract/PRB/v26/p614

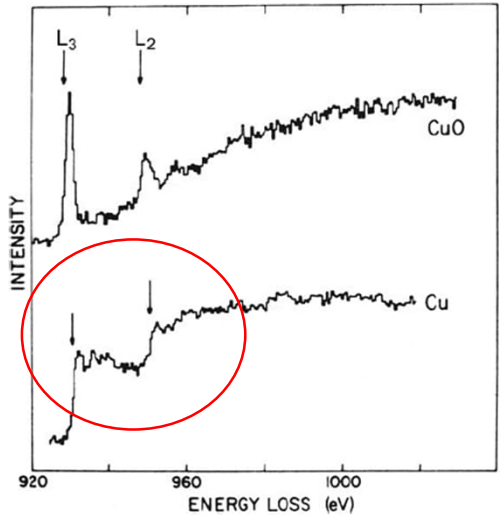

R.F. Egerton. Electron Energy-Loss Spectronscopy in the Electron Microscope

Chemistry

- Different elements create absorption edges at different energies, but the shapes are also determined by the bonding of the cations.
- The strong L-edge peaks are created by high density of vacant d-states
- In metallic Cu the d band is full and similar peaks are not seen
- In copper oxide the electrons are drawn away from the cation creating empty d-states and a strong L_3, and L_2 peaks

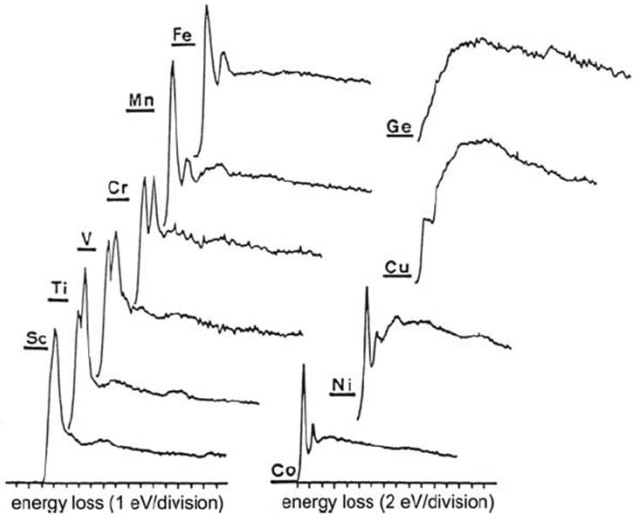

Fig. 3.45 *L*-edges of fourth-period elements measured using 120-keV electrons and a collection semi-angle of 5.7 mrad. From Zaluzec (1982), copyright Elsevier

Fig. 3.46 Cu L_{23} edges in metallic copper and in cupric oxide, measured using 75-keV electrons scattered up to $\beta = 2$ mrad. From Leapman et al. (1982), copyright American Physical Society. Available at http://link.aps.org/abstract/PRB/v26/p614

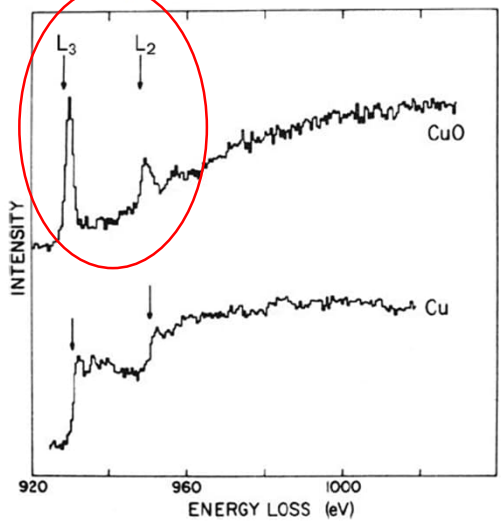

R.F. Egerton. Electron Energy-Loss Spectronscopy in the Electron Microscope

ELNES

- The energy-loss near-edge structure of an ionization edge represents approximately a local densities of states at the atom giving rise to the edge
- Able to determine CN and the symmetry of the nearest ligands

Fig. 5.37 Carbon *K*-edges of minerals containing the carbonate anion, an example of trigonal planar bonding, compared with the *K*-edges of elemental carbon. Spectra (energy resolution 0.5 eV) were deconvolved to remove plural scattering and peak distortion due to the asymmetrical energy distribution of the field-emission source. From Garvie et al. (1994), copyright Mineralogical Society of America, with permission

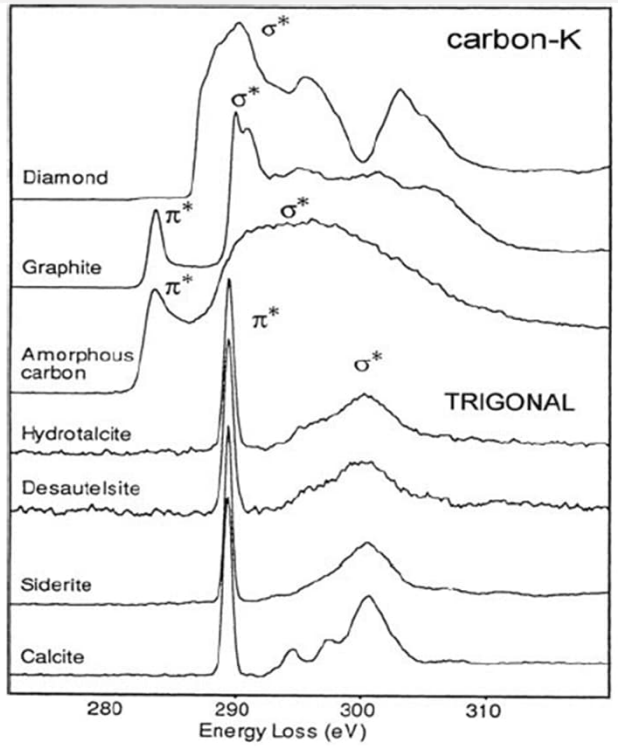

R.F. Egerton. Electron Energy-Loss Spectronscopy in the Electron Microscope

ELNES

- The energy-loss near-edge structure of an ionization edge represents approximately a local densities of states at the atom giving rise to the edge
- Able to determine CN and the symmetry of the nearest ligands
- Signal for a characteristic trigonal planar coordination of carbonates
- A sharp π* peak followed by a broader σ*

Fig. 5.37 Carbon *K*-edges of minerals containing the carbonate anion, an example of trigonal planar bonding, compared with the *K*-edges of elemental carbon. Spectra (energy resolution 0.5 eV) were deconvolved to remove plural scattering and peak distortion due to the asymmetrical energy distribution of the field-emission source. From Garvie et al. (1994), copyright Mineralogical Society of America, with permission

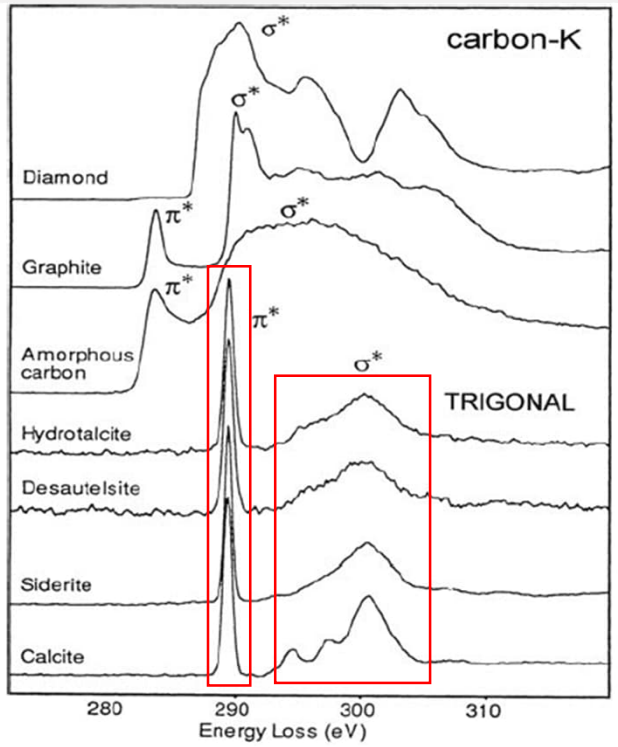

R.F. Egerton. Electron Energy-Loss Spectronscopy in the Electron Microscope

ELNES

- The energy-loss near-edge structure of an ionization edge represents approximately a local densities of states at the atom giving rise to the edge
- Able to determine CN and the symmetry of the nearest ligands
- Signal for a characteristic trigonal planar coordination of carbonates
- A sharp π* peak followed by a broader σ*
- A slightly different peak is seen in graphite and amorphous carbon, where the sp2 bonding is between other carbon atoms. Excitation: 1s -> π*

Fig. 5.37 Carbon *K*-edges of minerals containing the carbonate anion, an example of trigonal planar bonding, compared with the *K*-edges of elemental carbon. Spectra (energy resolution 0.5 eV) were deconvolved to remove plural scattering and peak distortion due to the asymmetrical energy distribution of the field-emission source. From Garvie et al. (1994), copyright Mineralogical Society of America, with permission

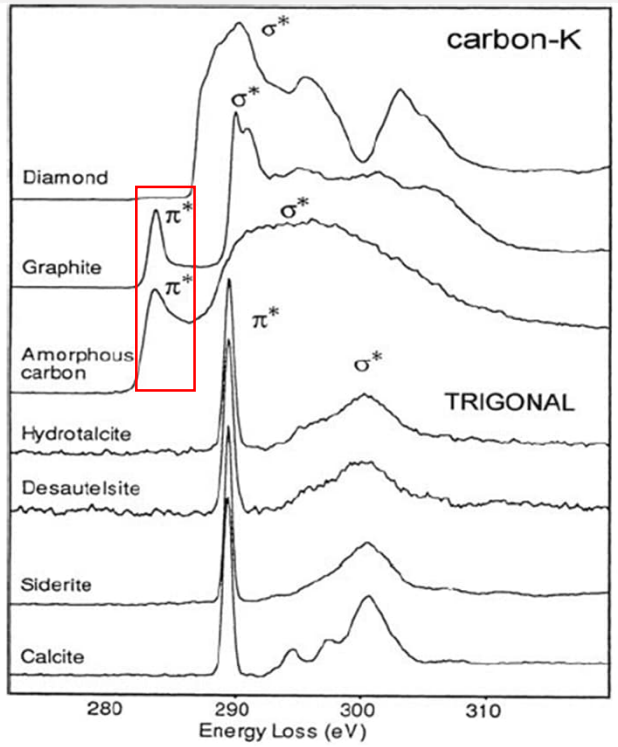

R.F. Egerton. Electron Energy-Loss Spectronscopy in the Electron Microscope

ELNES

- The energy-loss near-edge structure of an ionization edge represents approximately a local densities of states at the atom giving rise to the edge
- Able to determine CN and the symmetry of the nearest ligands
- Signal for a characteristic trigonal planar coordination of carbonates
- A sharp π* peak followed by a broader σ*
- A slightly different peak is seen in graphite and amorphous carbon, where the sp2 bonding is between other carbon atoms. Excitation: 1s -> π*
- The sp3 diamond bonds have no empty π* state so we do not see a similar K-edge

Fig. 5.37 Carbon *K*-edges of minerals containing the carbonate anion, an example of trigonal planar bonding, compared with the *K*-edges of elemental carbon. Spectra (energy resolution 0.5 eV) were deconvolved to remove plural scattering and peak distortion due to the asymmetrical energy distribution of the field-emission source. From Garvie et al. (1994), copyright Mineralogical Society of America, with permission

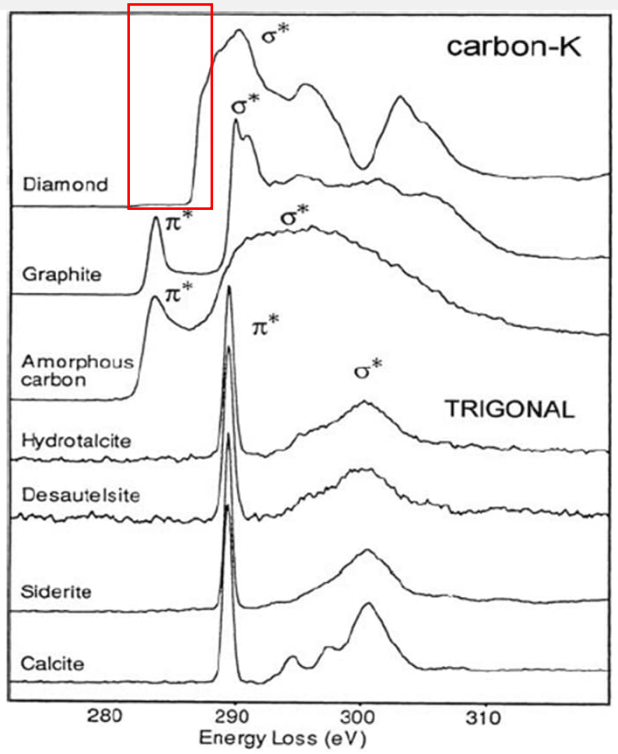

R.F. Egerton. Electron Energy-Loss Spectronscopy in the Electron Microscope

Type of information gained

- Structural and chemical information about solid materials
- Bonding and coordination number, mean oxidation state of cations
- Scattering of electrons, divided into elastic and inelastic scattering

Type of information gained

- Structural and chemical information about solid materials
- Bonding and coordination number, mean oxidation state of cations
- Scattering of electrons, divided into elastic and inelastic scattering
- Band structure and diaelectric properties of material
  (<50 eV, low-loss region)

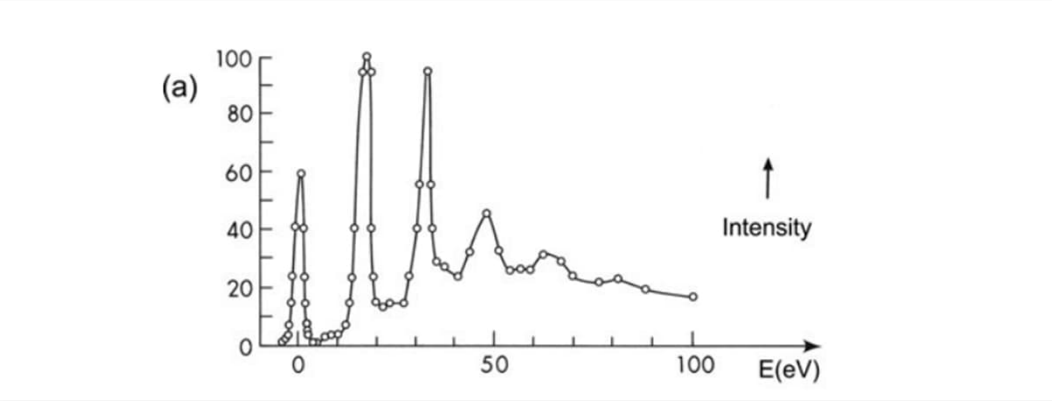

R.F. Egerton. Electron Energy-Loss Spectronscopy in the Electron Microscope

Type of information gained

- Structural and chemical information about solid materials
- Bonding and coordination number, mean oxidation state of cations
- Scattering of electrons, divided into elastic and inelastic scattering
- Band structure and diaelectric properties of material
  (<50 eV, low-loss region)
- Ionisation edges (>50 eV, high-loss region)

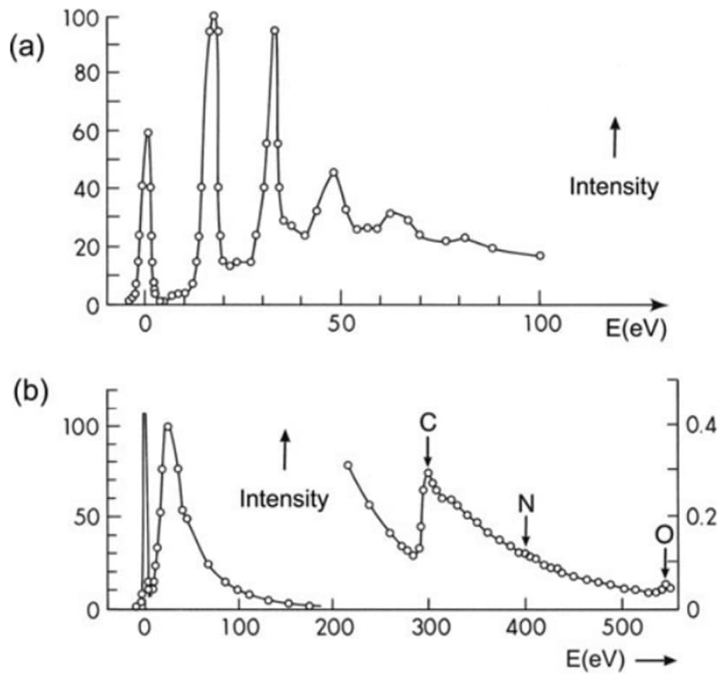

Fig. 1.7 (**a**) Energy-loss spectrum of 5.3-keV electrons transmitted through a thin foil of aluminum (Ruthemann, 1941), exhibiting plasmon peaks at multiples of 16 eV loss. (**b**) Energy-loss spectrum of 7.5-keV electrons transmitted through a thin film of collodion, showing *K*-ionization edges arising from carbon, nitrogen, and oxygen. Reprinted from Ruthemann (1941), copyright SpringerLink

R.F. Egerton. Electron Energy-Loss Spectronscopy in the Electron Microscope

Type of information gained

- Structural and chemical information about solid materials
- Bonding and coordination number, mean oxidation state of cations
- Scattering of electrons, divided into elastic and inelastic scattering
- Band structure and diaelectric properties of material (<50 eV, low-loss region)
- Ionisation edges (>50 eV, high-loss region)
- Capability to distinguish different allotropes of the same element

Fig. 5.63 (**a**) Low-loss and (**b**) *K*-loss spectra of fullerites, compared with graphite. From Kuzuo et al. (1994), copyright American Physical Society. http://link.aps.org/abstract/PRB/v49/p5054

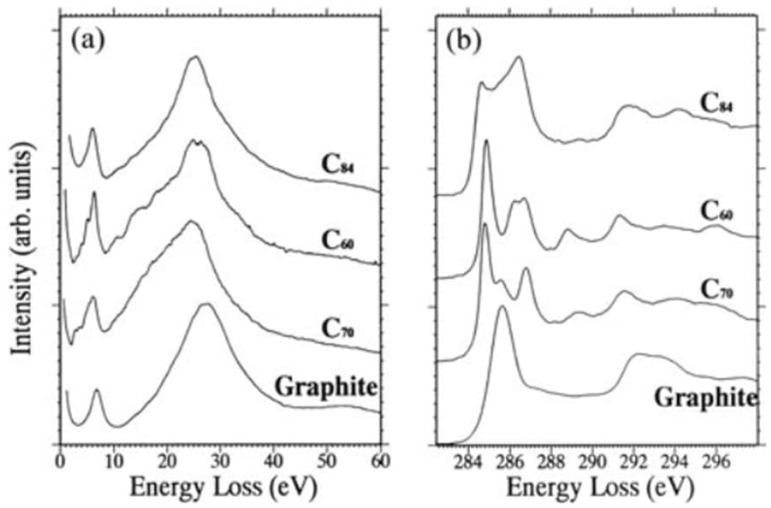

R.F. Egerton. Electron Energy-Loss Spectronscopy in the Electron Microscope

Advantages

- Very suitable for detection of light elements
- High energy resolution and few overlaps
- Can be combined with other methods, all in the same instrument
- Very fast technique (seconds to minutes)
- Standardless quantification

Advantages

- Very suitable for detection of light elements
- High energy resolution and few overlaps
- Can be combined with other methods, all in the same instrument
- Very fast technique (seconds to minutes)
- Standardless quantification

Limitations

- Signal-to-noise ratio of the elemental signal is low
- <70 nm thick specimen only
- Complex processing required

EELS vs EDS

- The Figure on the shows the benefits of the better energy resolution of the EELS compared to EDS (or EDX)
- In EDS the Cr (L-peak) and O (K-peak) peaks are partially overlapping, which makes identification and quantification of the elements more difficult
- In EELS, because of the better energy resolution, the ionization edges are resolved much better
- Other benefits of EELS: more than elemental information, higher sensitivity to most elements, fast (EDS can take hours)
- Benefit of EDS: data processing is simple

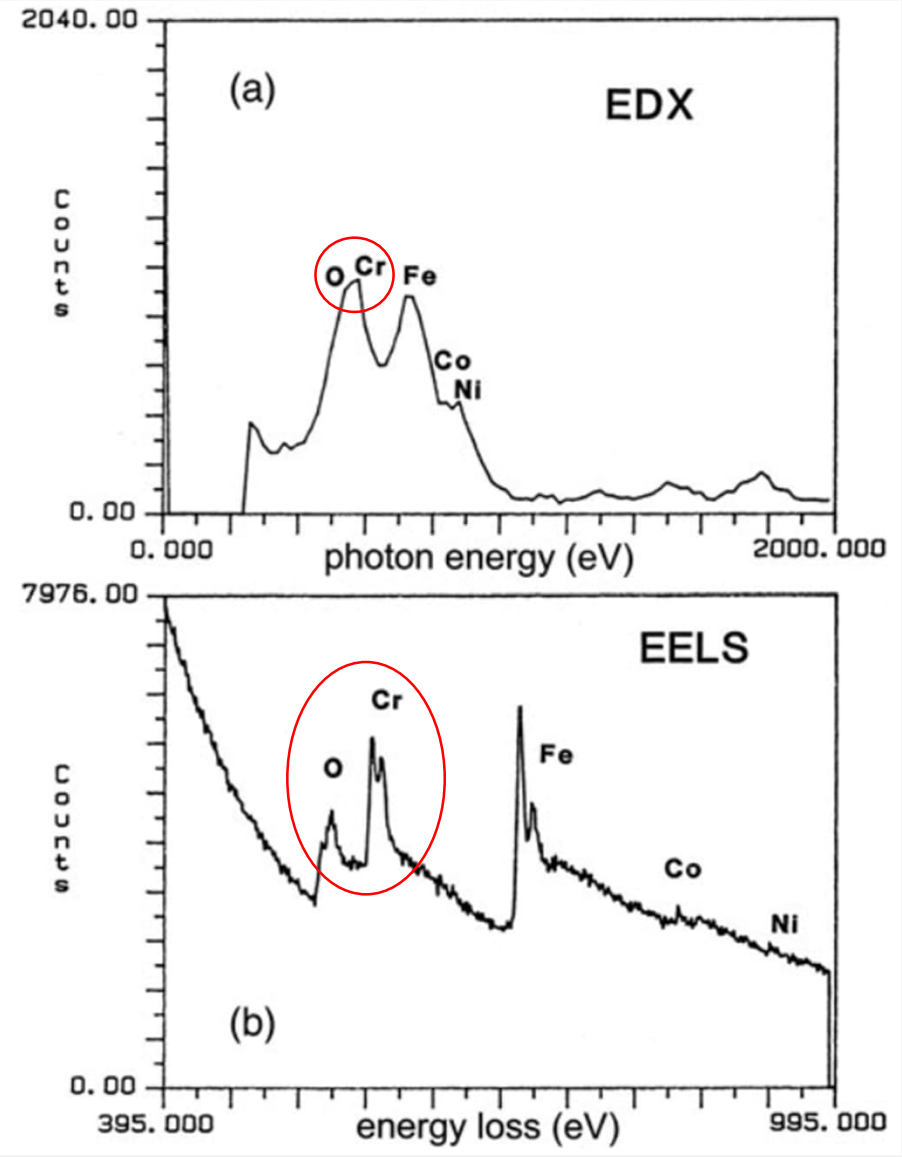

R.F. Egerton. Electron Energy-Loss Spectronscopy in the Electron Microscope

Research examples using EELS

Applied Surface Science 274 (2013) 195–202

Contents lists available at SciVerse ScienceDirect

Applied Surface Science

journal homepage: www.elsevier.com/locate/apsusc

Characterization of atomic structure of oxide films on carbon steel in simulated concrete pore solutions using EELS

H. Burak Gunay[a,1], Pouria Ghods[a], O. Burkan Isgor[a,*], Graham J.C. Carpenter[b], Xiaohua Wu[c]

[a] Carleton University, Department of Civil and Environmental Engineering, Ottawa, Canada
[b] CanmetMATERIALS, NRCan, Ottawa, Canada
[c] Natural Research Council of Canada, Information and Communications Technologies, Ottawa, Canada

ELSEVIER

Micron 37 (2006) 459–464

micron

www.elsevier.com/locate/micron

High resolution EELS of Cu–V oxides: Application to batteries materials

L. Laffont [a,*], M.Y. Wu [b], F. Chevallier [a], P. Poizot [a], M. Morcrette [a], J.M. Tarascon [a]

[a] Laboratoire de Reactivite et chimie des solides (LRCS), UMR 6007-CNRS, 33 rue Saint Leu, 80 039 AMIENS, France
[b] National Centre for HREM, Lorentz weg 1, 2628 CJ Delft, The Netherlands

Abstract

Although widely used, the most promising Li-based technologies still need to seek new materials concepts to satisfy the increasing demands for energy storage worldwide. We report a layered electrode material, $Cu_{2.33}V_4O_{11}$, for which the valency of copper, vanadium and thus indirectly the oxygen stoichiometry need to be investigated during the electrochemical cycle. High-resolution electron energy loss spectroscopy (HREELS) allows us to perform these measurements at the nanometer scale.

Keywords: HREELS; Cu and V valency; Batteries materials

1. Introduction

Electron energy loss spectroscopy (EELS), which enables the electronic density of states to be probed at a nanometer scale, is a powerful technique to study the chemical state of transition metal oxides in nano-powders or inhomo-

In this paper, we investigate the valency of copper and vanadium, i.e. indirectly the oxygen stoichiometry, in these materials at the nanometer scale during the electrochemical cycle by means of electron energy loss spectroscopy. The nanometer size of the powders, the questionable heterogeneity, as well as the need to examine crystallographic structure and

Dalton Transactions

ROYAL SOCIETY OF CHEMISTRY

PAPER

Check for updates

Cite this: *Dalton Trans.*, 2017, **46**, 4796

Atomic layer deposition of nickel–cobalt spinel thin films

D. J. Hagen, T. S. Tripathi and M. Karppinen *

We report the atomic layer deposition (ALD) of high-quality crystalline thin films of the spinel-oxide system $(Co_{1-x}Ni_x)_3O_4$. These spinel oxides are ferrimagnetic p-type semiconductors, and promising material candidates for several applications ranging from photovoltaics and spintronics to thermoelectrics. The spinel phase is obtained for Ni contents exceeding the $x = 0.33$ limit for bulk samples. It is observed that the electrical resistivity decreases continuously with x while the magnetic moment increases up to $x = 0.5$. This is in contrast to bulk samples where a decrease of resistivity is not observed for $x > 0.33$ due to the formation of a rock-salt phase. From UV-VIS-NIR absorption measurements, a change from distinct absorption edges for the parent oxide Co_3O_4 to a continuous absorption band ranging deep into the near infrared for $0 < x \leq 0.5$ was observed. The conformal deposition of dense films on high-aspect-ratio patterns is demonstrated.

Received 10th February 2017,
Accepted 16th March 2017

DOI: 10.1039/c7dt00512a

rsc.li/dalton

Gunay, H.B, Ghods, P., Isgor, B., Carpenter G.J.C. & Wu, X., Characterization of atomic structure of oxide films on carbon steel in simulated concrete pore solutions using EELS, Elsevier, Applied Surface Science

Laffont, L., Wu, M.Y., Chevallier, F., Poizot, P., Morcrette, M. & Tarascon, J.M., High resolution EELS of Cu–V oxides: Application to batteries materials

D.J. Hagen, T.S. Tripathi, and M. Karppinen, Atomic Layer Deposition of Nickel-Cobalt Spinel Thin Films, Dalton Transactions

Characterization of atomic structure of films

Applied Surface Science 274 (2013) 195–202

Contents lists available at SciVerse ScienceDirect

Applied Surface Science

journal homepage: www.elsevier.com/locate/apsusc

Characterization of atomic structure of oxide films on carbon steel in simulated concrete pore solutions using EELS

H. Burak Gunay[a,1], Pouria Ghods[a], O. Burkan Isgor[a,*], Graham J.C. Carpenter[b], Xiaohua Wu[c]

[a] Carleton University, Department of Civil and Environmental Engineering, Ottawa, Canada
[b] CanmetMATERIALS, NRCan, Ottawa, Canada
[c] Natural Research Council of Canada, Information and Communications Technologies, Ottawa, Canada

ARTICLE INFO

Article history:
Received 30 August 2012
Received in revised form 2 February 2013
Accepted 4 March 2013
Available online 14 March 2013

Keywords:
EELS
Passive film
Carbon steel rebar
Corrosion
Chloride
Concrete

ABSTRACT

The atomic structure of oxide films formed on carbon steel that are exposed to highly alkaline simulated concrete pore solutions was investigated using Electron Energy Loss Spectroscopy (EELS). In particular, the effect of chloride exposure on film structure was studied in two types of simulated pore solutions: saturated calcium hydroxide (CH) and a solution prepared to represent typical concrete pore solutions (CP). It was shown that the films that form on carbon steel in simulated concrete pore solutions contained three indistinct layers. The inner oxide film had a structure similar to that of $Fe^{II}O$, which is known to be unstable in the presence of chlorides. The outer oxide film mainly resembled Fe_3O_4 ($Fe^{II}O{\cdot}Fe_2{}^{III}O_3$) in the CH solution and α-$Fe_2{}^{III}O_3/Fe_3O_4$ in the CP solution. The composition of the transition layer between the inner and outer layers of the oxide film was mainly composed of Fe_3O_4 ($Fe^{II}O{\cdot}Fe_2{}^{III}O_3$). In the presence of chloride, the relative amount of the Fe^{III}/Fe^{II} increased, confirming that chlorides induce valence state transformation of oxides from Fe^{II} to Fe^{III}, and the difference between the atomic structures of oxide film layers diminished.

''Understanding the atomic structure of the oxide films that form on carbon steel is critical to explain passivity and chloride-induced depassivation processes in alkaline environments, particularly in concrete'' (Gunay H.B. et al)

Gunay, H.B, Ghods, P., Isgor, B., Carpenter G.J.C. & Wu, X., Characterization of atomic structure of oxide films on carbon steel in simulated concrete pore solutions using EELS, Elsevier, Applied Surface Science

Characterization of atomic structure of films

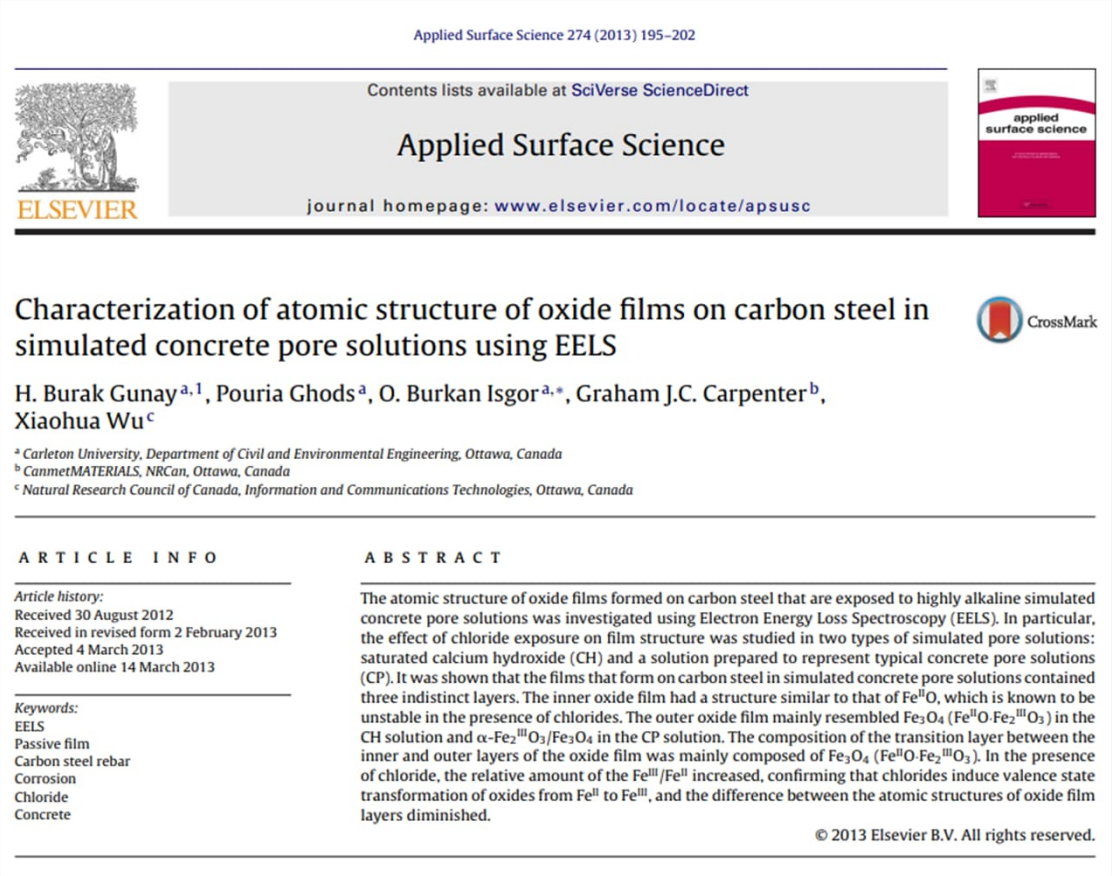

Applied Surface Science 274 (2013) 195–202

Contents lists available at SciVerse ScienceDirect

Applied Surface Science

journal homepage: www.elsevier.com/locate/apsusc

Characterization of atomic structure of oxide films on carbon steel in simulated concrete pore solutions using EELS

H. Burak Gunay[a,1], Pouria Ghods[a], O. Burkan Isgor[a,*], Graham J.C. Carpenter[b], Xiaohua Wu[c]

[a] Carleton University, Department of Civil and Environmental Engineering, Ottawa, Canada
[b] CanmetMATERIALS, NRCan, Ottawa, Canada
[c] Natural Research Council of Canada, Information and Communications Technologies, Ottawa, Canada

ARTICLE INFO

Article history:
Received 30 August 2012
Received in revised form 2 February 2013
Accepted 4 March 2013
Available online 14 March 2013

Keywords:
EELS
Passive film
Carbon steel rebar
Corrosion
Chloride
Concrete

ABSTRACT

The atomic structure of oxide films formed on carbon steel that are exposed to highly alkaline simulated concrete pore solutions was investigated using Electron Energy Loss Spectroscopy (EELS). In particular, the effect of chloride exposure on film structure was studied in two types of simulated pore solutions: saturated calcium hydroxide (CH) and a solution prepared to represent typical concrete pore solutions (CP). It was shown that the films that form on carbon steel in simulated concrete pore solutions contained three indistinct layers. The inner oxide film had a structure similar to that of $Fe^{II}O$, which is known to be unstable in the presence of chlorides. The outer oxide film mainly resembled Fe_3O_4 ($Fe^{II}O{\cdot}Fe_2{}^{III}O_3$) in the CH solution and α-$Fe_2{}^{III}O_3/Fe_3O_4$ in the CP solution. The composition of the transition layer between the inner and outer layers of the oxide film was mainly composed of Fe_3O_4 ($Fe^{II}O{\cdot}Fe_2{}^{III}O_3$). In the presence of chloride, the relative amount of the Fe^{III}/Fe^{II} increased, confirming that chlorides induce valence state transformation of oxides from Fe^{II} to Fe^{III}, and the difference between the atomic structures of oxide film layers diminished.

- Four carbon steel rebar samples
  - 2xCH: pH 12.5, Ca(OH)2
  - 2xCP: pH 13.3, Ca(OH)2, NaOH, KOH and Ca(SO4)
  - All samples were transferred to simulated concrete solution to form passive films
  - Two samples (CH-0, CP-0) before exposure to chloride and two samples (CH-1, CP-1) after exposure

Gunay, H.B, Ghods, P., Isgor, B., Carpenter G.J.C. & Wu, X., Characterization of atomic structure of oxide films on carbon steel in simulated concrete pore solutions using EELS, Elsevier, Applied Surface Science

Characterization of atomic structure of films

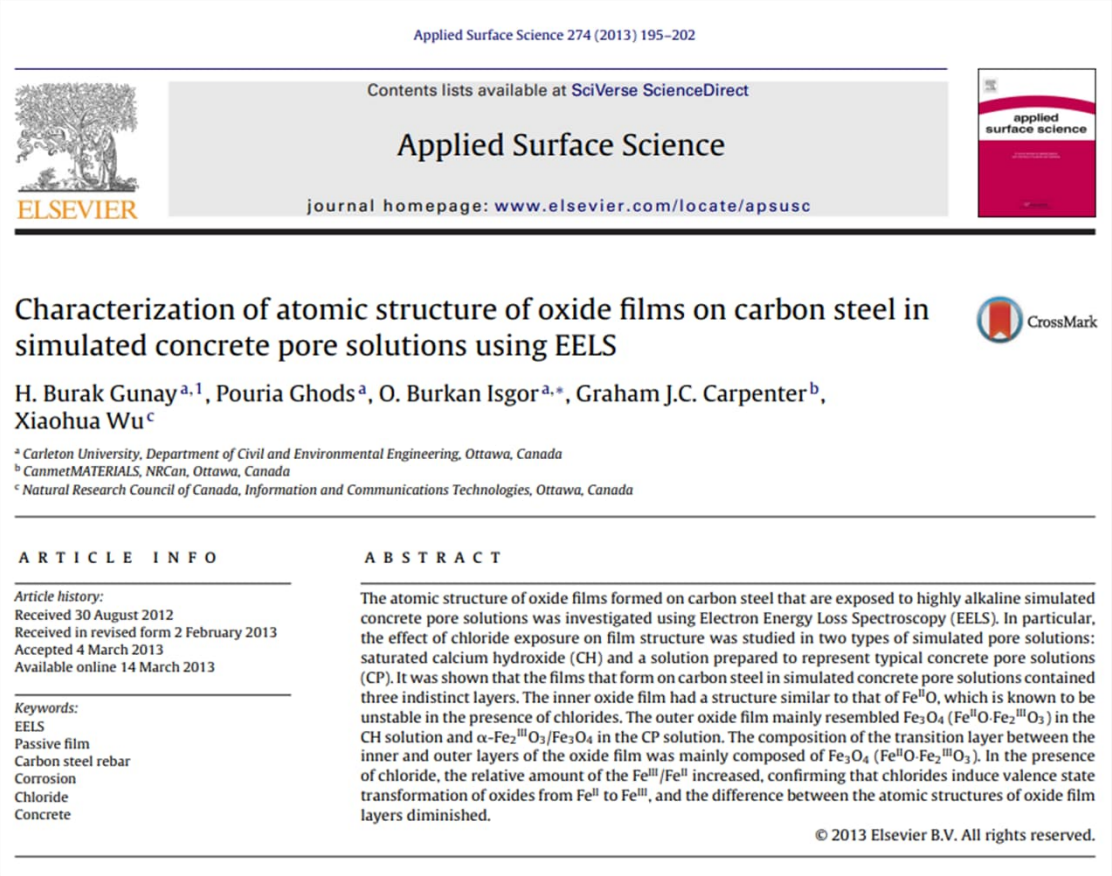

Applied Surface Science 274 (2013) 195–202

Contents lists available at SciVerse ScienceDirect

Applied Surface Science

journal homepage: www.elsevier.com/locate/apsusc

Characterization of atomic structure of oxide films on carbon steel in simulated concrete pore solutions using EELS

H. Burak Gunay[a,1], Pouria Ghods[a], O. Burkan Isgor[a,*], Graham J.C. Carpenter[b], Xiaohua Wu[c]

[a] Carleton University, Department of Civil and Environmental Engineering, Ottawa, Canada
[b] CanmetMATERIALS, NRCan, Ottawa, Canada
[c] Natural Research Council of Canada, Information and Communications Technologies, Ottawa, Canada

ARTICLE INFO

Article history:
Received 30 August 2012
Received in revised form 2 February 2013
Accepted 4 March 2013
Available online 14 March 2013

Keywords:
EELS
Passive film
Carbon steel rebar
Corrosion
Chloride
Concrete

ABSTRACT

The atomic structure of oxide films formed on carbon steel that are exposed to highly alkaline simulated concrete pore solutions was investigated using Electron Energy Loss Spectroscopy (EELS). In particular, the effect of chloride exposure on film structure was studied in two types of simulated pore solutions: saturated calcium hydroxide (CH) and a solution prepared to represent typical concrete pore solutions (CP). It was shown that the films that form on carbon steel in simulated concrete pore solutions contained three indistinct layers. The inner oxide film had a structure similar to that of $Fe^{II}O$, which is known to be unstable in the presence of chlorides. The outer oxide film mainly resembled Fe_3O_4 ($Fe^{II}O{\cdot}Fe_2{}^{III}O_3$) in the CH solution and α-$Fe_2{}^{III}O_3/Fe_3O_4$ in the CP solution. The composition of the transition layer between the inner and outer layers of the oxide film was mainly composed of Fe_3O_4 ($Fe^{II}O{\cdot}Fe_2{}^{III}O_3$). In the presence of chloride, the relative amount of the Fe^{III}/Fe^{II} increased, confirming that chlorides induce valence state transformation of oxides from Fe^{II} to Fe^{III}, and the difference between the atomic structures of oxide film layers diminished.

- Four carbon steel rebar samples
  - 2xCH: pH 12.5, Ca(OH)2
  - 2xCP: pH 13.3, Ca(OH)2, NaOH, KOH and Ca(SO4)
  - All samples were transferred to simulated concrete solution to form passive films
  - Two samples (CH-0, CP-0) before exposure to chloride and two samples (CH-1, CP-1) after exposure
- Atomic structure of inner, intermediate and outer oxide films were studied
  - Features of white lines (L-edge; L3 and L2, and O-edge)

Gunay, H.B, Ghods, P., Isgor, B., Carpenter G.J.C. & Wu, X., Characterization of atomic structure of oxide films on carbon steel in simulated concrete pore solutions using EELS, Elsevier, Applied Surface Science

Observations

- Fe-L2 peak intensity decreases relative to Fe-L3 peak from inner to outer oxide films
  - Differences between L3 peak relative to L2 is greater in CP-0 than CH-0

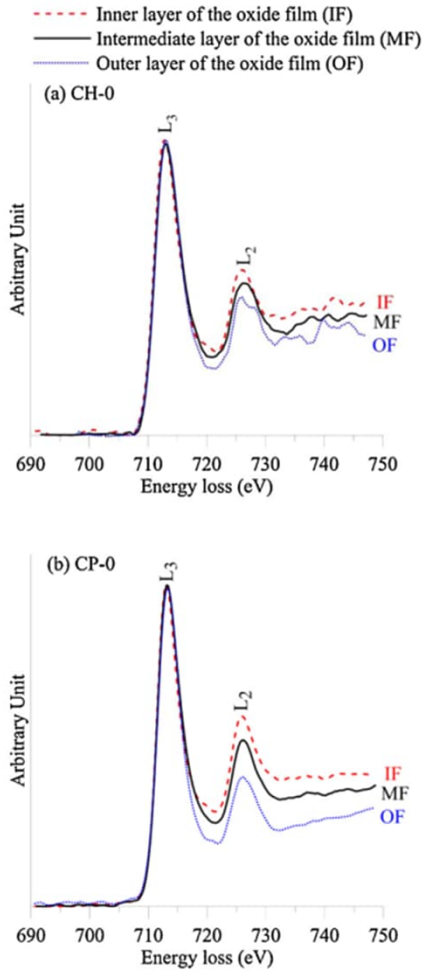

Fig. 4. Comparison of Fe-$L_{3,2}$ spectra at various depths of the oxide films formed in: (a) the CH solution (CH-0); (b) the CP solution (CP-0).

Gunay, H.B, Ghods, P., Isgor, B., Carpenter G.J.C. & Wu, X., Characterization of atomic structure of oxide films on carbon steel in simulated concrete pore solutions using EELS, Elsevier, Applied Surface Science

Observations

- Fe-L2 peak intensity decreases relative to Fe-L3 peak from inner to outer oxide films
  - Differences between L3 peak relative to L2 is greater in CP-0 than CH-0
- O-K pre-peaks relative intensity to main peak decreases from outer to inner oxide film
  - Oxidation states change for both from Fe(II) to Fe(III) from inner to outer layer

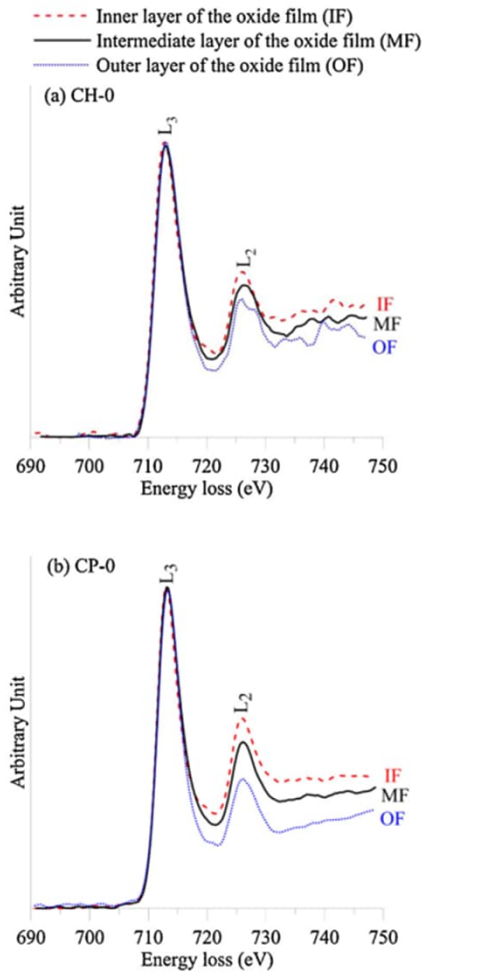

Fig. 4. Comparison of Fe-$L_{3,2}$ spectra at various depths of the oxide films formed in: (a) the CH solution (CH-0); (b) the CP solution (CP-0).

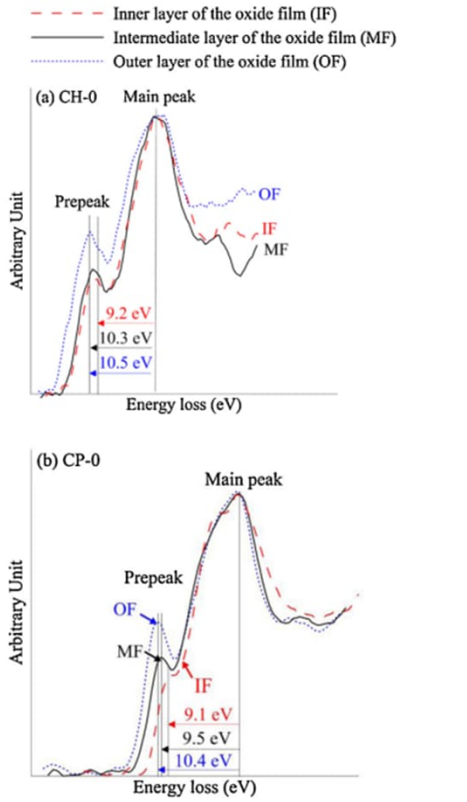

Fig. 5. Comparison of O-K spectra at various depths of the oxide films formed in (a) the CH solution (CH-0), (b) the CP solution (CP-0).

Gunay, H.B, Ghods, P., Isgor, B., Carpenter G.J.C. & Wu, X., Characterization of atomic structure of oxide films on carbon steel in simulated concrete pore solutions using EELS, Elsevier, Applied Surface Science

Observations

- Fe-L2 peak intensity decreases relative to Fe-L3 peak from inner to outer oxide films
  - Differences between L3 peak relative to L2 is greater in CP-0 than CH-0
- O-K pre-peaks relative intensity to main peak decreases from outer to inner oxide film
  - Oxidation states change for both from Fe(II) to Fe(III) from inner to outer layer
- Variation of atomic structure of oxide films is higher in CP-0 than in CH-0 based on the intensity ratio of L3/L2 and pre-peak/main peak

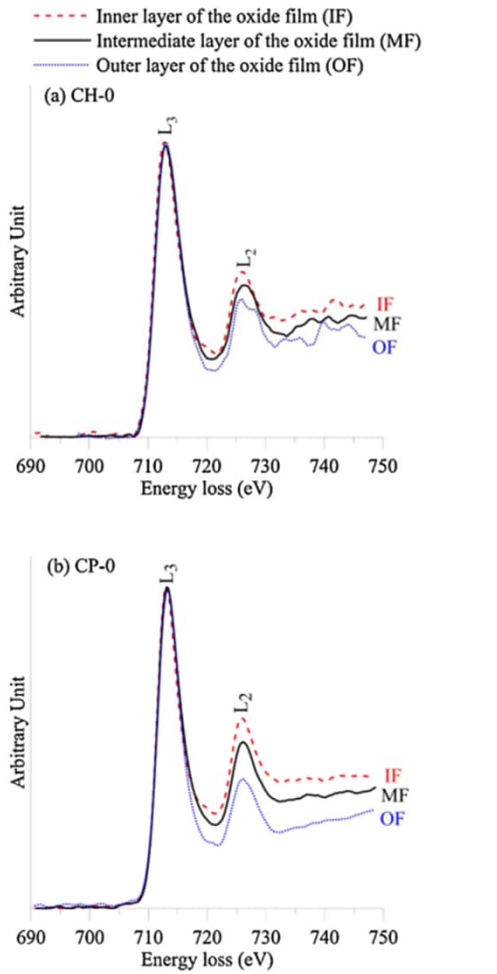

Fig. 4. Comparison of Fe-$L_{3,2}$ spectra at various depths of the oxide films formed in: (a) the CH solution (CH-0); (b) the CP solution (CP-0).

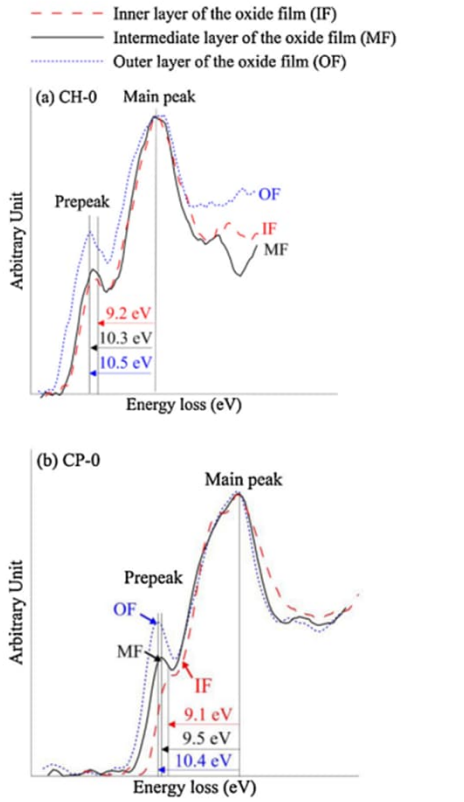

Fig. 5. Comparison of O-K spectra at various depths of the oxide films formed in (a) the CH solution (CH-0), (b) the CP solution (CP-0).

Gunay, H.B, Ghods, P., Isgor, B., Carpenter G.J.C. & Wu, X., Characterization of atomic structure of oxide films on carbon steel in simulated concrete pore solutions using EELS, Elsevier, Applied Surface Science

Results

- Fingerprints of different compositions can be used when determining the atomic structure of oxide layers
  - Fingerprints are calculated using the intensity ratio between L3 and L2 peaks

Table 4
Summary of fingerprints acquired from signature curves.

Fingerprints	Fe-$I(L_3)/I(L_2)$ (±0.3)	Δ (O-$K_{peak,pre\text{-}peak}$) (eV) (±0.2)	O-$I(K_{pre\text{-}peak})/I(K_{main\text{-}peak})$ (±0.01)
[a]Fe	3.8	N/A	N/A
[a]FeO	4.6	9	0.09
[a]Fe_3O_4	5.2	10.7	0.15
[a]γ-Fe_2O_3	5.8	10.9	0.2
[a]α-Fe_2O_3	6.5	11	0.2
[b]FeOOH	7.1	9.7	0.2
[c]β-FeOOH	7.1	9.5	0.2

[a] Colliex et al. [1].
[b] CEMES [10].
[c] NIST [9].

Table 5
Summary of fingerprints acquired from the results presented in Fig. 4 to Fig. 7.

Specimen		Fingerprints			Iron oxide match
		Fe-$I(L_3)/I(L_2)$ (±0.3)	Δ(O-$K_{peak,prepeak}$) (eV) (±0.2)	O-$I(K_{prepeak})/I(K_{peak})$ (±0.01)	
Inner oxide film	CH-0	4.3	9.2	0.11	FeO
	CH-1	6.1	9.5	0.17	γ-Fe_2O_3/β-FeOOH
	CP-0	4.2	9.1	0.07	FeO
	CP-1	4.3	9.0	0.10	FeO
Mid-oxide film	CH-0	4.7	10.3	0.12	FeO/Fe_3O_4
	CH-1	7.6	9.4	0.20	FeOOH
	CP-0	5.5	9.5	0.14	FeO/Fe_3O_4
	CP-1	4.9	9.0	0.12	FeO/β-FeOOH
Outer oxide film	CH-0	5.4	10.5	0.15	Fe_3O_4
	CH-1	7.5	10.6	0.21	FeOOH
	CP-0	6.9	10.4	0.19	Fe_3O_4/α-Fe_2O_3
	CP-1	5.3	9.6	0.16	Fe_3O_4/FeOOH

Gunay, H.B, Ghods, P., Isgor, B., Carpenter G.J.C. & Wu, X., Characterization of atomic structure of oxide films on carbon steel in simulated concrete pore solutions using EELS, Elsevier, Applied Surface Science

Results

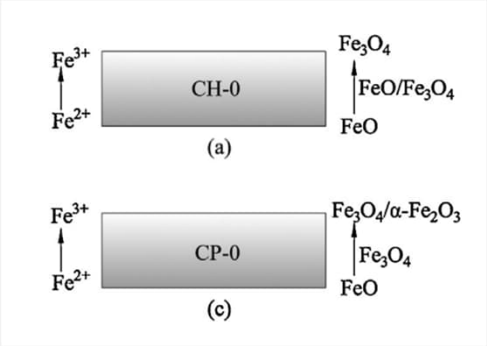

- Fingerprints of different compositions can be used when determining the atomic structure of oxide layers
  - Fingerprints are calculated using the intensity ratio between L3 and L2 peaks
- Concrete pore solution affects the atomic structure of oxide layers
  - CH-0 and CP-0 both are composed of inner layer of FeO, known to be protective alkaline media
  - Intermediate layer contains some traces of Fe3O4 (Fe(II) ions occupy half of the octahedral sites and Fe(III) the other half and tetrahedral sites)
  - CH-0 outer layer contains Fe3O4 and CP-0 Fe3O4 and some traces of α-Fe2O3

Gunay, H.B, Ghods, P., Isgor, B., Carpenter G.J.C. & Wu, X., Characterization of atomic structure of oxide films on carbon steel in simulated concrete pore solutions using EELS, Elsevier, Applied Surface Science

Results

- Fingerprints of different compositions can be used when determining the atomic structure of oxide layers
  - Fingerprints are calculated using the intensity ratio between L3 and L2 peaks

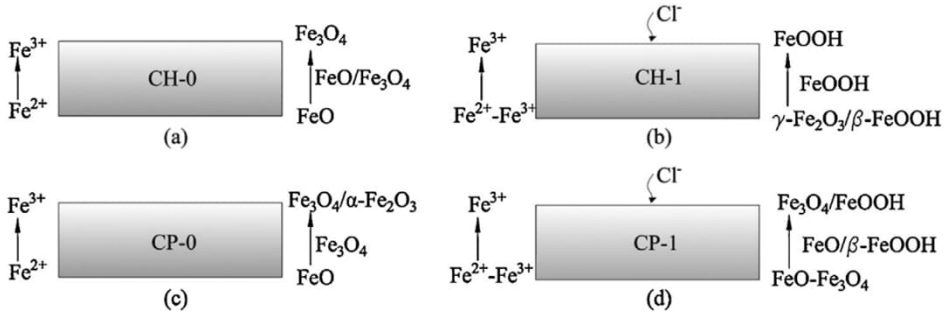

Fig. 8. The schematic representation of the chemical composition and the changes in the oxidation state of the oxide films in: (a) the CH-0 specimen; (b) the CH-1specimen; (c) the CP-0 specimen; (d) the CP-1 specimen.

- Concrete pore solution affects the atomic structure of oxide layers
  - CH-0 and CP-0 both are composed of inner layer of FeO, known to be protective alkaline media
  - Intermediate layer contains some traces of Fe3O4 (Fe(II) ions occupy half of the octahedral sites and Fe(III) the other half and tetrahedral sites)
  - CH-0 outer layer contains Fe3O4 and CP-0 Fe3O4 and some traces of α-Fe2O3
- Exposure to chloride variates the chemical composition
  - CH-1 inner layer contains γ-Fe2O3 and β-FeOOH and CP-1 addition to FeO, some traces of Fe3O4
  - Outer layers were uneffected

Gunay, H.B, Ghods, P., Isgor, B., Carpenter G.J.C. & Wu, X., Characterization of atomic structure of oxide films on carbon steel in simulated concrete pore solutions using EELS, Elsevier, Applied Surface Science

Valency of elements in compound

ELSEVIER

Micron 37 (2006) 459–464

micron

www.elsevier.com/locate/micron

High resolution EELS of Cu–V oxides: Application to batteries materials

L. Laffont [a,*], M.Y. Wu [b], F. Chevallier [a], P. Poizot [a], M. Morcrette [a], J.M. Tarascon [a]

[a] *Laboratoire de Reactivite et chimie des solides (LRCS), UMR 6007-CNRS, 33 rue Saint Leu, 80 039 AMIENS, France*
[b] *National Centre for HREM, Lorentz weg 1, 2628 CJ Delft, The Netherlands*

Abstract

Although widely used, the most promising Li-based technologies still need to seek new materials concepts to satisfy the increasing demands for energy storage worldwide. We report a layered electrode material, $Cu_{2.33}V_4O_{11}$, for which the valency of copper, vanadium and thus indirectly the oxygen stoichiometry need to be investigated during the electrochemical cycle. High-resolution electron energy loss spectroscopy (HREELS) allows us to perform these measurements at the nanometer scale.

Keywords: HREELS; Cu and V valency; Batteries materials

1. Introduction

Electron energy loss spectroscopy (EELS), which enables the electronic density of states to be probed at a nanometer scale, is a powerful technique to study the chemical state of transition metal oxides in nano-powders or inhomo-

In this paper, we investigate the valency of copper and vanadium, i.e. indirectly the oxygen stoichiometry, in these materials at the nanometer scale during the electrochemical cycle by means of electron energy loss spectroscopy. The nanometer size of the powders, the questionable heterogeneity, as well as the need to examine crystallographic structure and

''Investigation of the valency of copper and vanadium, that is indirectly the oxygen stoichiometry, in these materials at the nanometer scale during the electrochemical cycle''
(Laffont, L. et al)

Laffont, L., Wu, M.Y., Chevallier, F., Poizot, P., Morcrette, M. & Tarascon, J.M., High resolution EELS of Cu–V oxides: Application to batteries materials

Valency of elements in compound

ELSEVIER

Micron 37 (2006) 459–464

micron

www.elsevier.com/locate/micron

High resolution EELS of Cu–V oxides: Application to batteries materials

L. Laffont [a,*], M.Y. Wu [b], F. Chevallier [a], P. Poizot [a], M. Morcrette [a], J.M. Tarascon [a]

[a] *Laboratoire de Reactivite et chimie des solides (LRCS), UMR 6007-CNRS, 33 rue Saint Leu, 80 039 AMIENS, France*
[b] *National Centre for HREM, Lorentz weg 1, 2628 CJ Delft, The Netherlands*

Abstract

Although widely used, the most promising Li-based technologies still need to seek new materials concepts to satisfy the increasing demands for energy storage worldwide. We report a layered electrode material, $Cu_{2.33}V_4O_{11}$, for which the valency of copper, vanadium and thus indirectly the oxygen stoichiometry need to be investigated during the electrochemical cycle. High-resolution electron energy loss spectroscopy (HREELS) allows us to perform these measurements at the nanometer scale.

Keywords: HREELS; Cu and V valency; Batteries materials

1. Introduction

Electron energy loss spectroscopy (EELS), which enables the electronic density of states to be probed at a nanometer scale, is a powerful technique to study the chemical state of transition metal oxides in nano-powders or inhomo-

In this paper, we investigate the valency of copper and vanadium, i.e. indirectly the oxygen stoichiometry, in these materials at the nanometer scale during the electrochemical cycle by means of electron energy loss spectroscopy. The nanometer size of the powders, the questionable heterogeneity, as well as the need to examine crystallographic structure and

- Usage of high resolution EELS (HREELS)
- Powdered Cu2.333V4O11 was prepared
  - From stoichiometric amounts of Cu2O, V2O5 and V2O4 oxides
- Performed in argon filled dry box
  - Li metal as negative and reference electrode
  - Saturated with 1 M LiPF6 in ethylene carbonate-dimethyl carbonate as the electrolyte
  - Composite electrode disk of Cu2.33V4O11, mixed with 15% of carbon used as positive electrode

Laffont, L., Wu, M.Y., Chevallier, F., Poizot, P., Morcrette, M. & Tarascon, J.M., High resolution EELS of Cu–V oxides: Application to batteries materials

Valency of elements in compound

ELSEVIER

Micron 37 (2006) 459–464

micron

www.elsevier.com/locate/micron

High resolution EELS of Cu–V oxides: Application to batteries materials

L. Laffont [a,*], M.Y. Wu [b], F. Chevallier [a], P. Poizot [a], M. Morcrette [a], J.M. Tarascon [a]

[a] *Laboratoire de Reactivite et chimie des solides (LRCS), UMR 6007-CNRS, 33 rue Saint Leu, 80 039 AMIENS, France*
[b] *National Centre for HREM, Lorentz weg 1, 2628 CJ Delft, The Netherlands*

Abstract

Although widely used, the most promising Li-based technologies still need to seek new materials concepts to satisfy the increasing demands for energy storage worldwide. We report a layered electrode material, $Cu_{2.33}V_4O_{11}$, for which the valency of copper, vanadium and thus indirectly the oxygen stoichiometry need to be investigated during the electrochemical cycle. High-resolution electron energy loss spectroscopy (HREELS) allows us to perform these measurements at the nanometer scale.

Keywords: HREELS; Cu and V valency; Batteries materials

1. Introduction

Electron energy loss spectroscopy (EELS), which enables the electronic density of states to be probed at a nanometer scale, is a powerful technique to study the chemical state of transition metal oxides in nano-powders or inhomo-

In this paper, we investigate the valency of copper and vanadium, i.e. indirectly the oxygen stoichiometry, in these materials at the nanometer scale during the electrochemical cycle by means of electron energy loss spectroscopy. The nanometer size of the powders, the questionable heterogeneity, as well as the need to examine crystallographic structure and

- Usage of high resolution EELS (HREELS)
- Powdered Cu2.333V4O11 was prepared
  - From stoichiometric amounts of Cu2O, V2O5 and V2O4 oxides
- Performed in argon filled dry box
  - Li metal as negative and reference electrode
  - Saturated with 1 M LiPF6 in ethylene carbonate-dimethyl carbonate as the electrolyte
  - Composite electrode disk of Cu2.33V4O11, mixed with 15% of carbon used as positive electrode
- Charge distribution of Cu and V cations was studied by comparing obtained data to simulated spectra
- Two samples were prepared but only one discussed now

Laffont, L., Wu, M.Y., Chevallier, F., Poizot, P., Morcrette, M. & Tarascon, J.M., High resolution EELS of Cu–V oxides: Application to batteries materials

Observations

- Simulated V-L2,3 and O-K edges spectra
  - V2O3, VO2 and V2O5 used for reference spectra of V(III), V(IV) V(V)
- Simulated O-K edge for oxygen
  - The change in the edge is due to a rigid shift of valence band as the oxidation changes from V(V) to V(III)

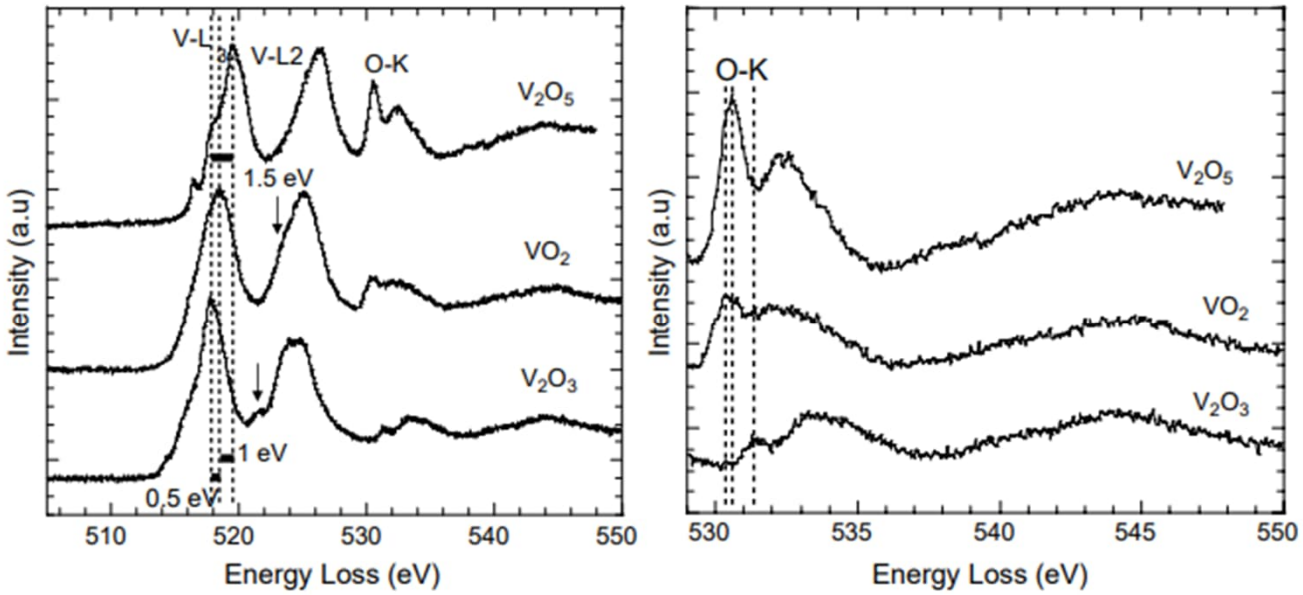

Fig. 1. Comparison between the V-$L_{2,3}$ and O-K HREELS spectra of reference oxides.

Laffont, L., Wu, M.Y., Chevallier, F., Poizot, P., Morcrette, M. & Tarascon, J.M., High resolution EELS of Cu–V oxides: Application to batteries materials

Observations

- Simulated V-L2,3 and O-K edges spectra
  - V2O3, VO2 and V2O5 used for reference spectra of V(III), V(IV) V(V)
- Simulated O-K edge for oxygen
  - The change in the edge is due to a rigid shift of valence band as the oxidation changes from V(V) to V(III)
- Simulated Cu-L2,3 edges
  - CuO, Cu2O and Cu used for reference spectra of Cu(II), Cu(I) and Cu(0)

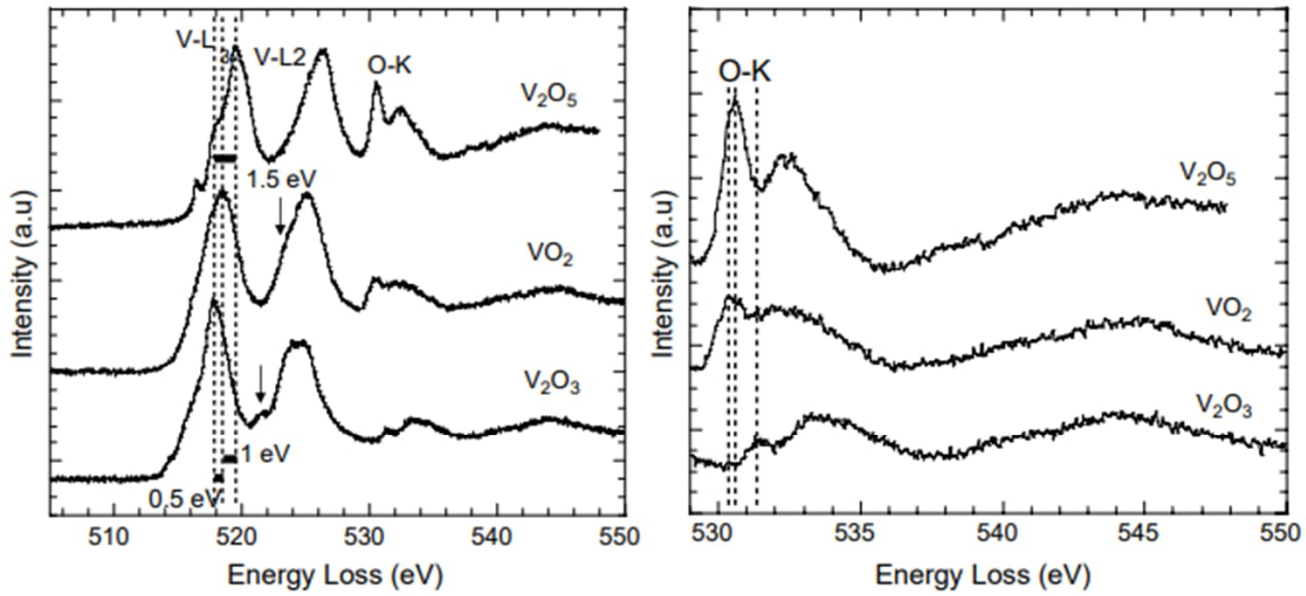

Fig. 1. Comparison between the V-$L_{2,3}$ and O-K HREELS spectra of reference oxides.

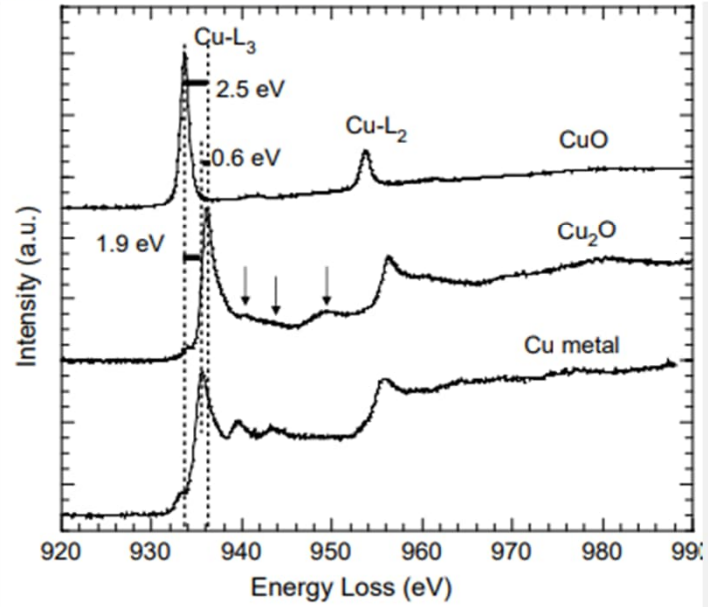

Fig. 2. Comparison between the Cu-$L_{2,3}$ spectra of reference oxides.

Laffont, L., Wu, M.Y., Chevallier, F., Poizot, P., Morcrette, M. & Tarascon, J.M., High resolution EELS of Cu–V oxides: Application to batteries materials

Observations

- Simulated V-L2,3 and O-K edges spectra
  - V2O3, VO2 and V2O5 used for reference spectra of V(III), V(IV) V(V)
- Simulated O-K edge for oxygen
  - The change in the edge is due to a rigid shift of valence band as the oxidation changes from V(V) to V(III)
- Simulated Cu-L2,3 edges
  - CuO, Cu2O and Cu used for reference spectra of Cu(II), Cu(I) and Cu(0)
- Possible redox couples are Cu(II)/Cu(I), V(V)/V(IV), V(IV)/V(III) as well for Cu metal
- Valences are observed at the end of first phase transition and at the end of second phase transition

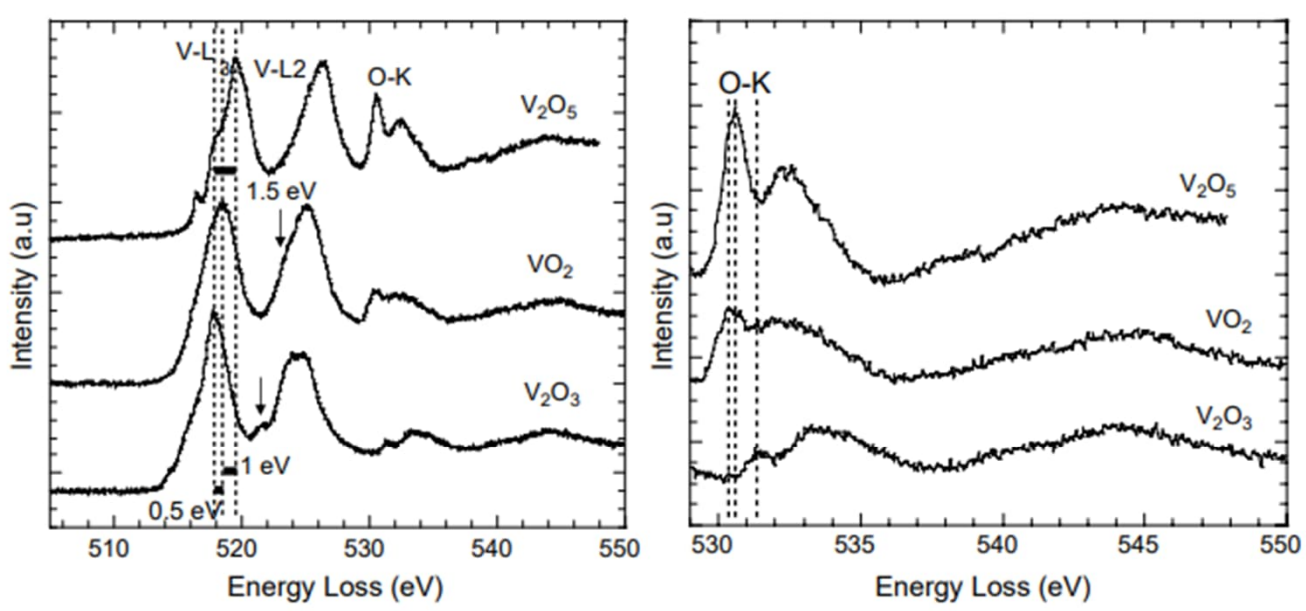

Fig. 1. Comparison between the V-$L_{2,3}$ and O-K HREELS spectra of reference oxides.

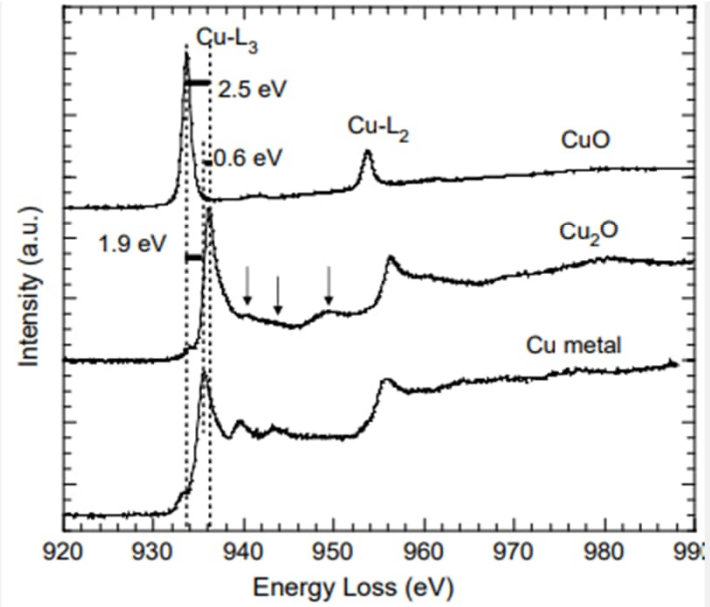

Fig. 2. Comparison between the Cu-$L_{2,3}$ spectra of reference oxides.

Laffont, L., Wu, M.Y., Chevallier, F., Poizot, P., Morcrette, M. & Tarascon, J.M., High resolution EELS of Cu–V oxides: Application to batteries materials

Results

End of the first phase transition

- Possible redox couple V(V)/V(IV)
  - Energy position of samples L3 indicates V2O3 L3 edge
  - Energy position of samples L3 and L2 indicate V2O5 edge
- However, Cu-L2,3 matches with divalent copper and the redox couple is then Cu(I)/Cu(0)

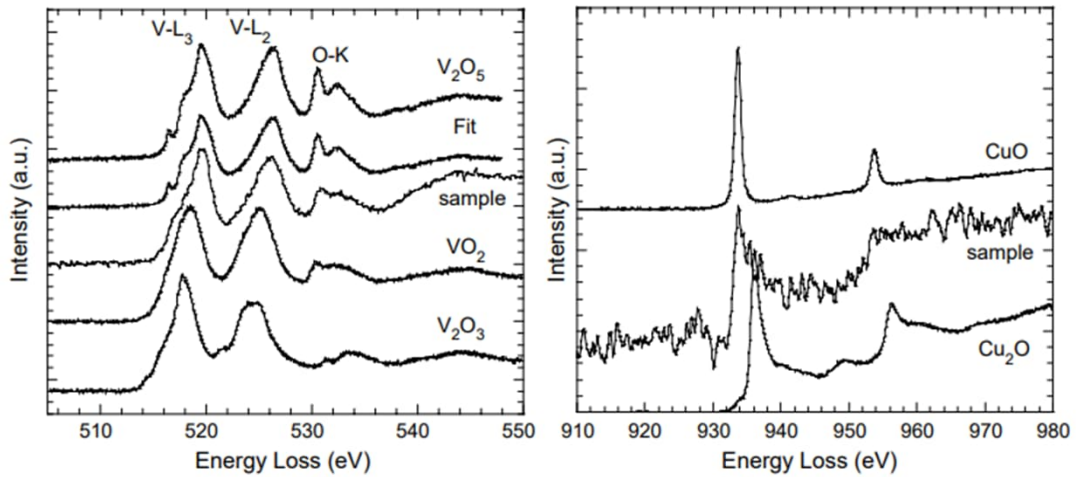

Fig. 4. ELNES of the V-$L_{2,3}$ edges of the reference vanadium oxides and the $Cu_{2.33}V_4O_{11}$ discharged at $x=2.2$ Li (experimental and simulated) and comparison between the Cu-$L_{2,3}$ spectra of reference copper oxides and the sample studied.

Laffont, L., Wu, M.Y., Chevallier, F., Poizot, P., Morcrette, M. & Tarascon, J.M., High resolution EELS of Cu–V oxides: Application to batteries materials

Results

End of the first phase transition

- Possible redox couple V(V)/V(IV)
  - Energy position of samples L3 indicates V2O3 L3 edge
  - Energy position of samples L3 and L2 indicate V2O5 edge
- However, Cu-L2,3 matches with divalent copper and the redox couple is then Cu(I)/Cu(0)

End of the second phase transition

- Redox couple V(V)/V(IV)
  - Energy position matches to VO2 and shape to V2O5
- No signal detected from copper
  - Only small fraction of Cu(II) is present and most of it was transformed to Cu metal
  - Redox couple Cu(II)/Cu(0)

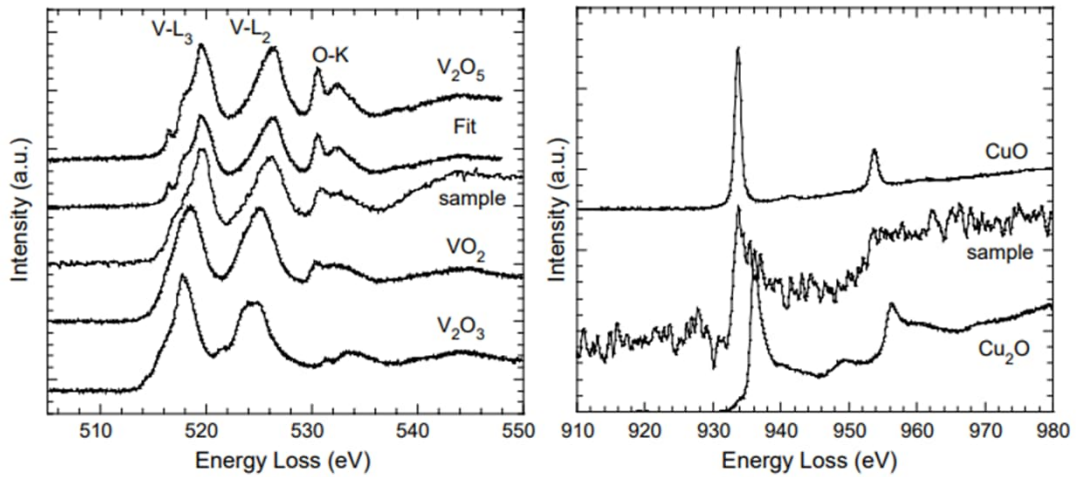

Fig. 4. ELNES of the V-$L_{2,3}$ edges of the reference vanadium oxides and the $Cu_{2.33}V_4O_{11}$ discharged at $x=2.2$ Li (experimental and simulated) and comparison between the Cu-$L_{2,3}$ spectra of reference copper oxides and the sample studied.

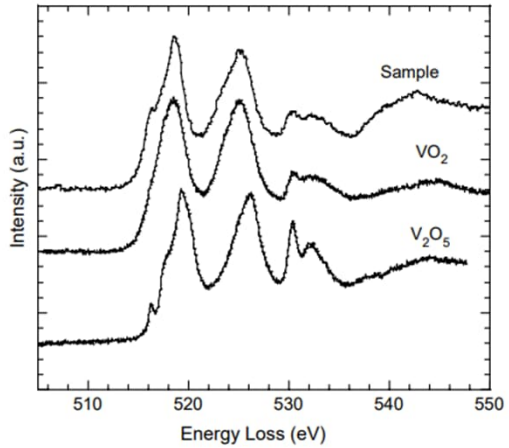

Fig. 5. Comparison between the V-$L_{2,3}$ spectra of the $Cu_{2.33}V_4O_{11}$ discharged at $x=4.9$ Li and the reference vanadium oxides.

Laffont, L., Wu, M.Y., Chevallier, F., Poizot, P., Morcrette, M. & Tarascon, J.M., High resolution EELS of Cu–V oxides: Application to batteries materials

EELS as an Additional Analytical Tool

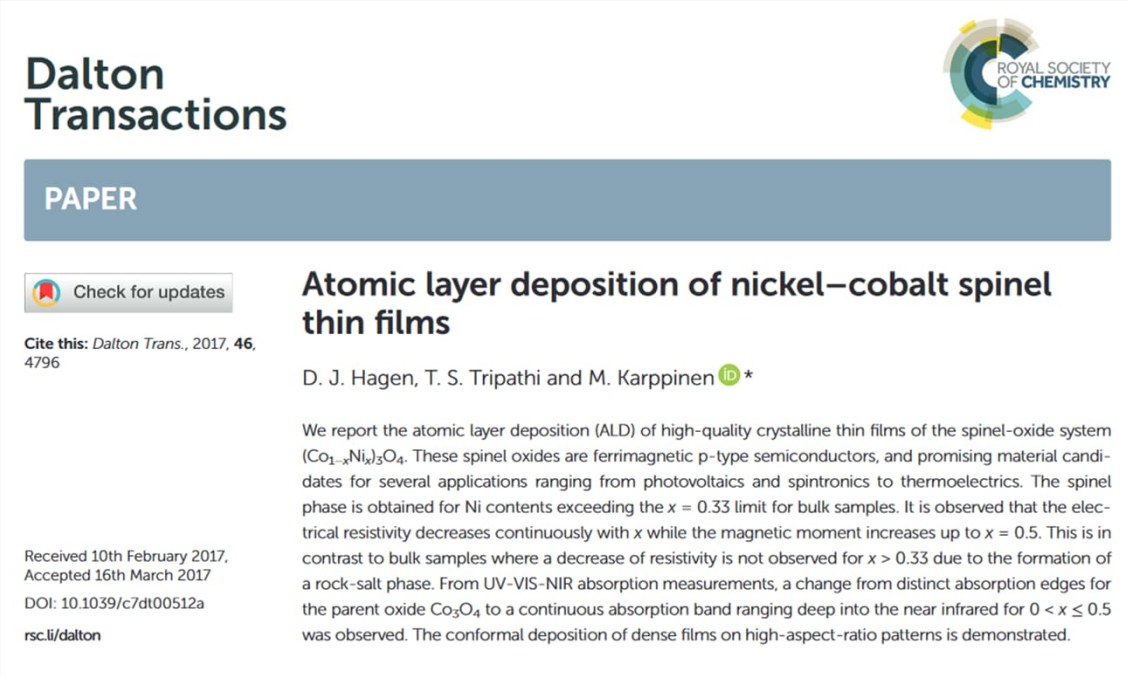

Dalton Transactions

ROYAL SOCIETY OF CHEMISTRY

PAPER

Check for updates

Cite this: *Dalton Trans.*, 2017, **46**, 4796

Atomic layer deposition of nickel–cobalt spinel thin films

D. J. Hagen, T. S. Tripathi and M. Karppinen *

We report the atomic layer deposition (ALD) of high-quality crystalline thin films of the spinel-oxide system $(Co_{1-x}Ni_x)_3O_4$. These spinel oxides are ferrimagnetic p-type semiconductors, and promising material candidates for several applications ranging from photovoltaics and spintronics to thermoelectrics. The spinel phase is obtained for Ni contents exceeding the $x = 0.33$ limit for bulk samples. It is observed that the electrical resistivity decreases continuously with x while the magnetic moment increases up to $x = 0.5$. This is in contrast to bulk samples where a decrease of resistivity is not observed for $x > 0.33$ due to the formation of a rock-salt phase. From UV-VIS-NIR absorption measurements, a change from distinct absorption edges for the parent oxide Co_3O_4 to a continuous absorption band ranging deep into the near infrared for $0 < x \leq 0.5$ was observed. The conformal deposition of dense films on high-aspect-ratio patterns is demonstrated.

Received 10th February 2017,
Accepted 16th March 2017

DOI: 10.1039/c7dt00512a

rsc.li/dalton

- Atomic layer deposition (ALD) of p-type semiconductor spinel oxides $(Co_{1-x}Ni_x)_3O_4$
- Study uses multiple different characterization techniques, EELS being one of them
- Thermoelectric, electric, optical, and magnetic properties of the films are studied

D.J. Hagen, T.S. Tripathi, and M. Karppinen, Atomic Layer Deposition of Nickel-Cobalt Spinel Thin Films, Dalton Transactions, 2017, 46, 4796.

EELS as an Additional Analytical Tool

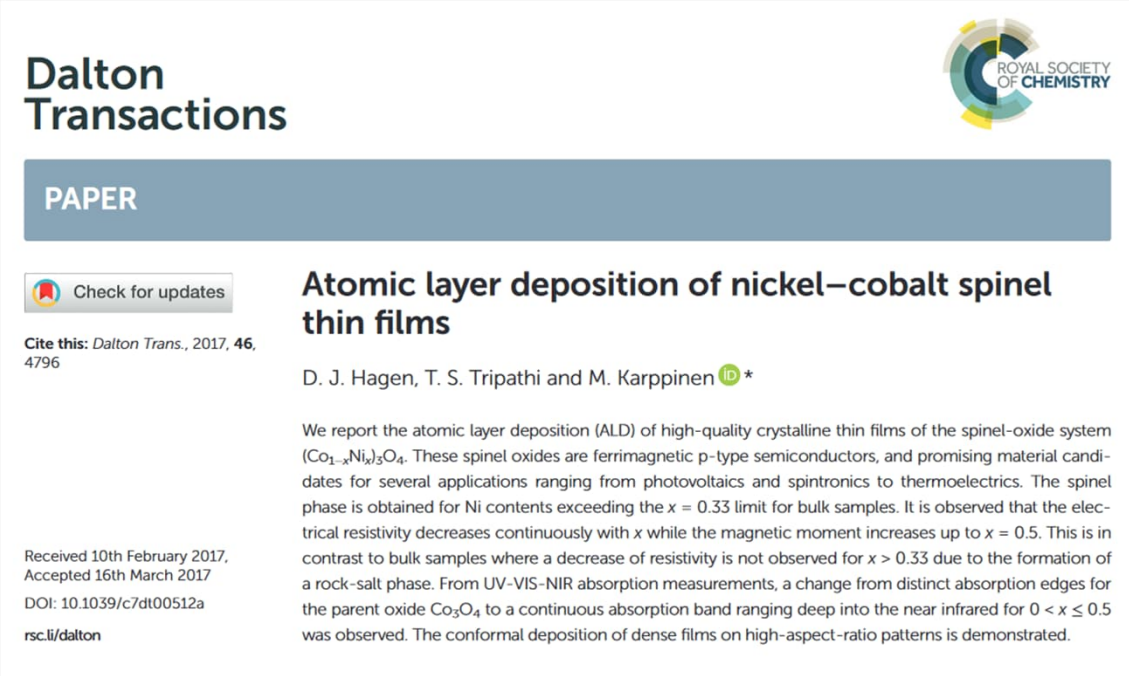

Dalton Transactions

ROYAL SOCIETY OF CHEMISTRY

PAPER

Check for updates

Cite this: *Dalton Trans.*, 2017, **46**, 4796

Atomic layer deposition of nickel–cobalt spinel thin films

D. J. Hagen, T. S. Tripathi and M. Karppinen *

We report the atomic layer deposition (ALD) of high-quality crystalline thin films of the spinel-oxide system $(Co_{1-x}Ni_x)_3O_4$. These spinel oxides are ferrimagnetic p-type semiconductors, and promising material candidates for several applications ranging from photovoltaics and spintronics to thermoelectrics. The spinel phase is obtained for Ni contents exceeding the $x = 0.33$ limit for bulk samples. It is observed that the electrical resistivity decreases continuously with x while the magnetic moment increases up to $x = 0.5$. This is in contrast to bulk samples where a decrease of resistivity is not observed for $x > 0.33$ due to the formation of a rock-salt phase. From UV-VIS-NIR absorption measurements, a change from distinct absorption edges for the parent oxide Co_3O_4 to a continuous absorption band ranging deep into the near infrared for $0 < x \leq 0.5$ was observed. The conformal deposition of dense films on high-aspect-ratio patterns is demonstrated.

Received 10th February 2017,
Accepted 16th March 2017

DOI: 10.1039/c7dt00512a

rsc.li/dalton

D.J. Hagen, T.S. Tripathi, and M. Karppinen, Atomic Layer Deposition of Nickel-Cobalt Spinel Thin Films, Dalton Transactions, 2017, 46, 4796.

- Atomic layer deposition (ALD) of p-type semiconductor spinel oxides $(Co_{1-x}Ni_x)_3O_4$
- Study uses multiple different characterization techniques, EELS being one of them
- Thermoelectric, electric, optical, and magnetic properties of the films are studied
- Thickness of the film was investigated using X-ray reflection (XRR)
- Gracing incident x-ray diffraction (GIXRD) and TEM was used to study the crystal structure
- Films were prepared using focused ion beam (FIG)
- Chemical composition was studied using lithium-drifted silicon EDS and EELS equipped with omega type filter

Observations

- ALD precursors: ($Ni(tmhd)_2$) and ($Co(tmhd)_2$)
- Growth per cycle (GPC) as a function of ($Co(tmhd)_2$) pulse length. Saturation at relatively low pulse length

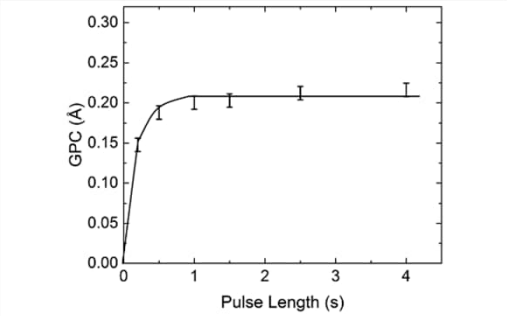

Fig. 1 GPC as a function of $Co(tmhd)_2$ pulse length for a Co_3O_4 film at a deposition temperature of 200 °C for a fixed O_3 pulse length of 3 s.

D.J. Hagen, T.S. Tripathi, and M. Karppinen, Atomic Layer Deposition of Nickel-Cobalt Spinel Thin Films, Dalton Transactions, 2017, 46, 4796.

Observations

- ALD precursors: ($Ni(tmhd)_2$) and ($Co(tmhd)_2$)
- Growth per cycle (GPC) as a function of ($Co(tmhd)_2$) pulse length. Saturation at relatively low pulse length
- GIXRD of $(Co_{1-x}Ni_x)_3O_4$: Ni endmember crystallizes in rock-salt structure and Co endmember in spinel structure

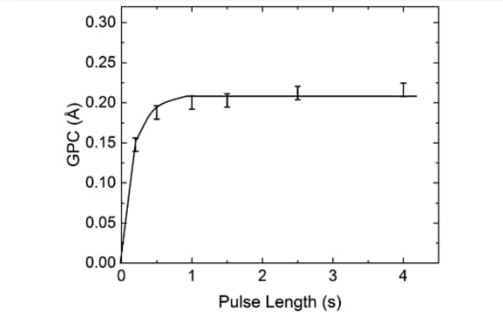

Fig. 1 GPC as a function of $Co(tmhd)_2$ pulse length for a Co_3O_4 film at a deposition temperature of 200 °C for a fixed O_3 pulse length of 3 s.

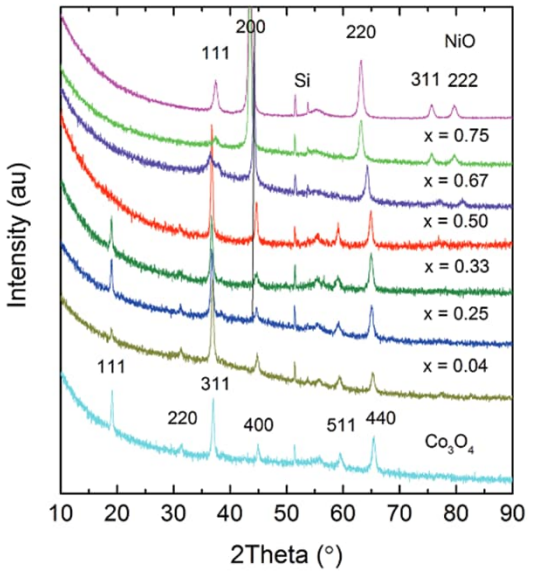

Fig. 2 XRD patterns of $(Co_{1-x}Ni_x)_3O_4$ films with different Ni contents x. The Miller indices are for the parent oxides, Co_3O_4 and NiO.

D.J. Hagen, T.S. Tripathi, and M. Karppinen, Atomic Layer Deposition of Nickel-Cobalt Spinel Thin Films, Dalton Transactions, 2017, 46, 4796.

Observations

- ALD precursors: ($Ni(tmhd)_2$) and ($Co(tmhd)_2$)
- Growth per cycle (GPC) as a function of ($Co(tmhd)_2$) pulse length. Saturation at relatively low pulse length
- GIXRD of $(Co_{1-x}Ni_x)_3O_4$: Ni endmember crystallizes in rock-salt structure and Co endmember in spinel structure
- TEM images (a) low-magnification, (b) high-magnification showing grain boundaries, (c) diffraction pattern
- (d) EDS of the profile

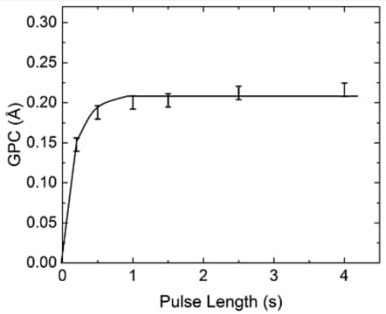

Fig. 1 GPC as a function of $Co(tmhd)_2$ pulse length for a Co_3O_4 film at a deposition temperature of 200 °C for a fixed O_3 pulse length of 3 s.

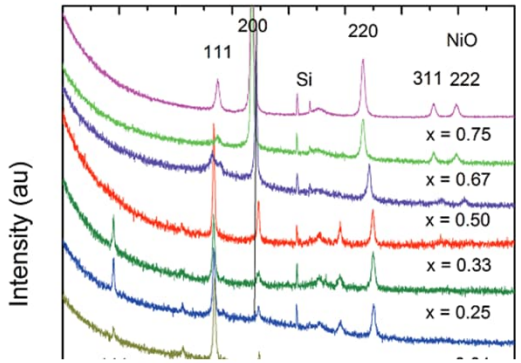

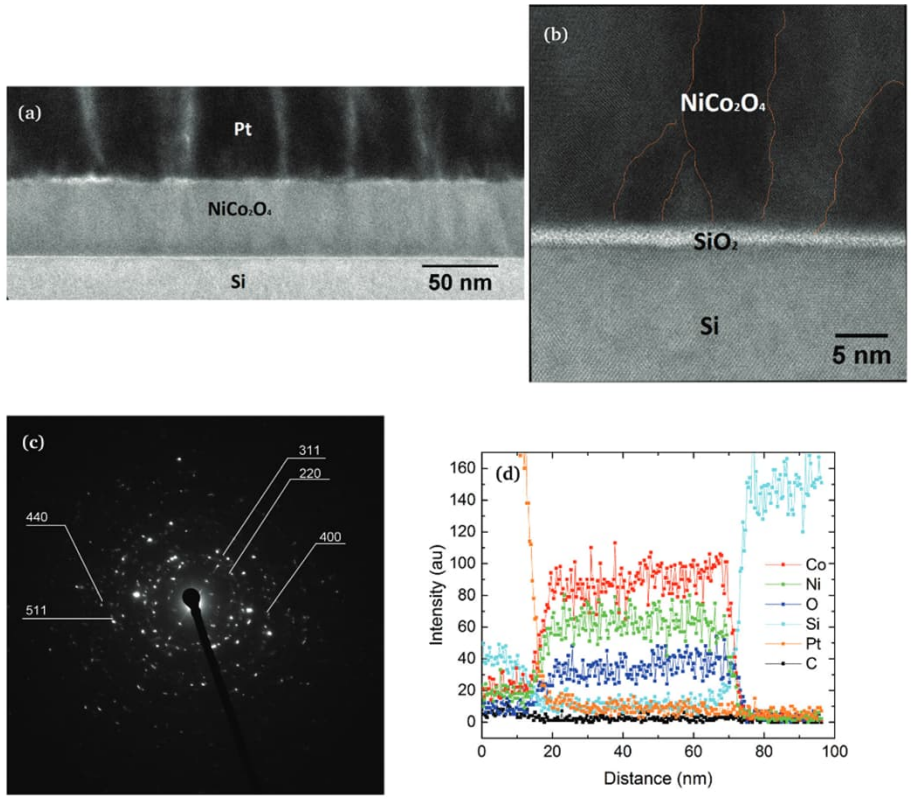

Fig. 3 TEM analysis of a representative $(Co_{1-x}Ni_x)_3O_4$ film (x = 0.33): (a) low-magnification image, (b) high-magnification image (some grain boundaries are indicated), (c) selected-area electron diffraction pattern, (d) elemental profile measured with EDS.

D.J. Hagen, T.S. Tripathi, and M. Karppinen, Atomic Layer Deposition of Nickel-Cobalt Spinel Thin Films, Dalton Transactions, 2017, 46, 4796.

Observations

- EELS was used to detect the mean oxidation state of the metal cations using the L_2 and L_3 peaks
- The excitation of the inner shell electrons (mostly 2p to 3d for the first-row transition metals) cause the characteristic peaks whose ratio (L_3/L_2) can be used to characterize the oxidation state of the metal cations:
- Co^{2+}: 4.8
- $Co^{2.67+}$ (Co_3O_4): 3.3
- After subtracting the background, the ratio was determined to be 3.5 and the oxidation state of Co lower than 3+
- The result shows that there is a deviation from an ideal inverse spinel

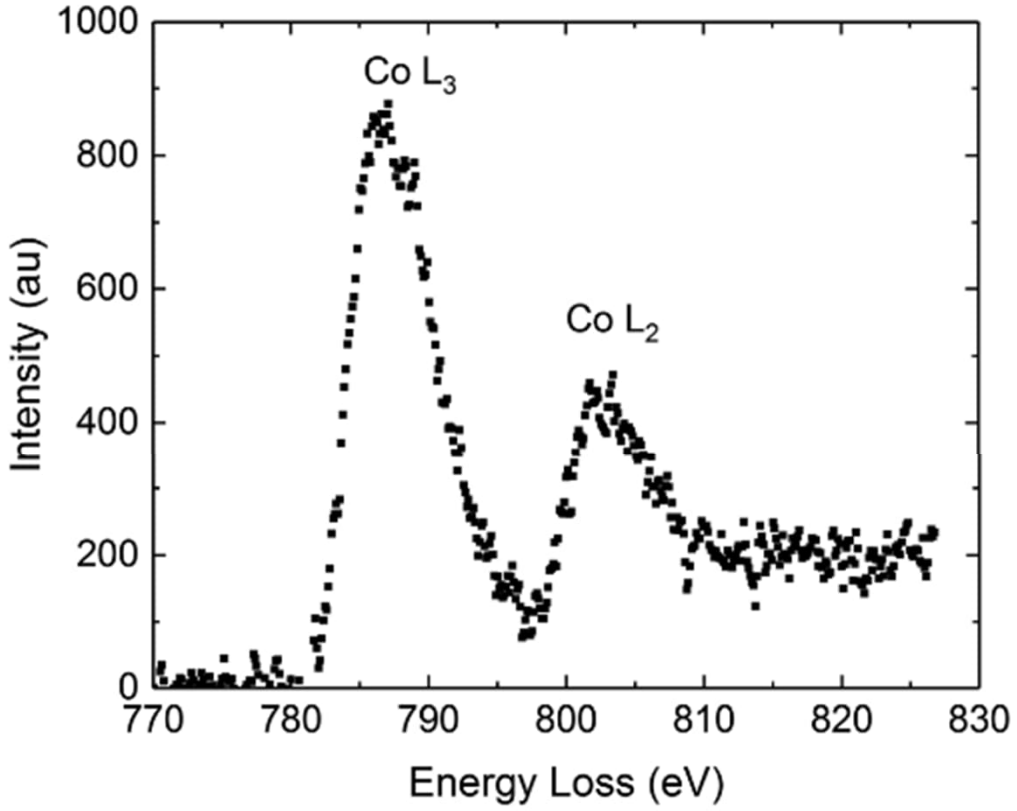

Fig. 4 EELS graph for the $(Co_{1-x}Ni_x)_3O_4$ film with $x = 0.33$: the ratio of the Co L_3 and L_2 peaks strongly indicates a valence lower than +3.

D.J. Hagen, T.S. Tripathi, and M. Karppinen, Atomic Layer Deposition of Nickel-Cobalt Spinel Thin Films, Dalton Transactions, 2017, 46, 4796.

Other Methods and Conclusions

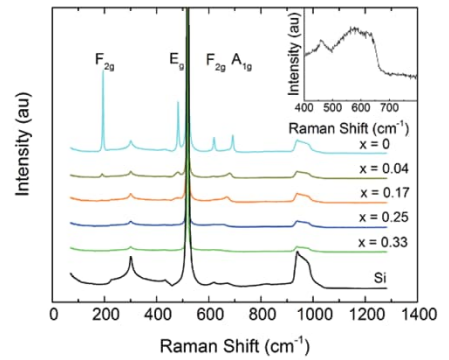

Fig. 5 Raman spectra for $(Co_{1-x}Ni_x)_3O_4$ films with different Ni contents x. The inset shows the Raman spectrum for a film with $x = 0.33$ and a thickness of 192 nm in higher resolution.

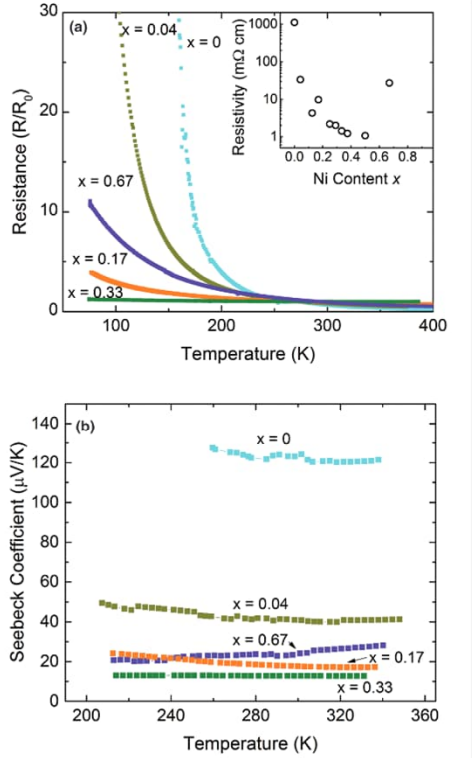

Fig. 6 Thermoelectric properties of $(Co_{1-x}Ni_x)_3O_4$ films: (a) resistance change with temperature; the resistance has been normalized to the value measured at 273 K. The inset shows the RT resistivity values depending on the Ni content x. (b) Temperature dependence of the Seebeck coefficient.

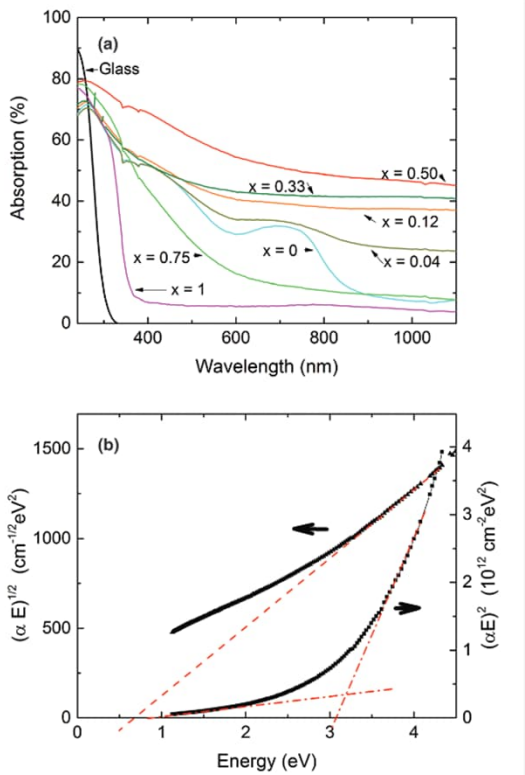

Fig. 7 UV-VIS-NIR absorption spectra: (a) absorption as a function of wavelength for $(Co_{1-x}Ni_x)_3O_4$ films with varying Ni contents x; (b) $(\alpha E)^2 - E$ and $(\alpha E)^{1/2} - E$ characteristic for a film with $x = 0.33$.

4. Conclusions

High-quality ternary oxide $(Co_{1-x}Ni_x)_3O_4$ thin films spanning the whole composition range between Co_3O_4 and NiO were deposited by ALD for the first time. For films with Ni/(Co + Ni) ratios x ranging from 0 to 0.5, the dominant phase was of spinel type as proven by XRD while only for the higher Ni contents NiO was formed. This is an advantage compared to bulk materials for which the rock-salt structure is dominant for $x > 0.33$. Within the spinel-type region, electrical resistivity decreases with increasing Ni content. The resistivities of spinel films with Co contents of the stoichiometric composition $(Co_{2/3}Ni_{1/3})_3O_4$ (0.0014 Ω cm) and less (0.00107 Ω cm) were much lower than that of bulk $(Co_{2/3}Ni_{1/3})_3O_4$ and comparable to $(Co_{2/3}Ni_{1/3})_3O_4$ films prepared by PVD (0.003 Ω cm, Windisch *et al.*[20]) and laser-ablation epitaxy (0.00083 Ω cm, Bitla *et al.*[19]). These low resistivities increase the thermoelectric power factor of Co_3O_4 overcompensating the decrease of the Seebeck coefficient due to the doping.

D.J. Hagen, T.S. Tripathi, and M. Karppinen, Atomic Layer Deposition of Nickel-Cobalt Spinel Thin Films, Dalton Transactions, 2017, 46, 4796.

Other Methods and Conclusions

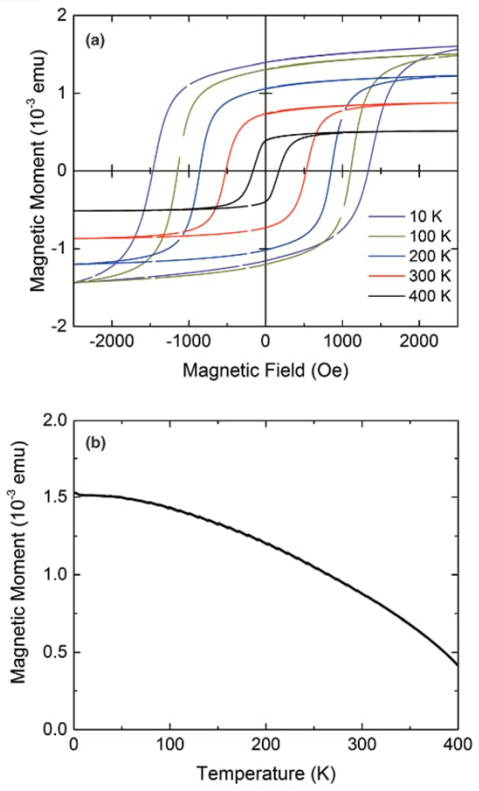

Fig. 8 Magnetic characterization of a $(Co_{1-x}Ni_x)_3O_4$ film with $x = 0.33$ (deposited with 9600 cycles): (a) saturation curves at various temperatures; (b) magnetic moment *vs.* temperature under a field of 2000 Oe.

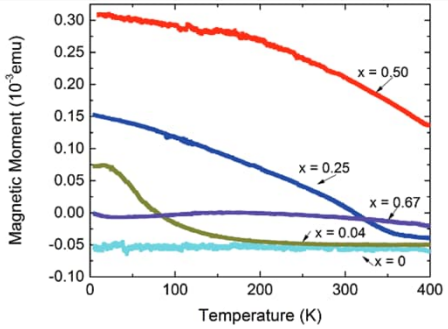

Fig. 9 Magnetic moment *vs.* temperature under a field of 10 kOe for $(Co_{1-x}Ni_x)_3O_4$ films with different Ni contents x. The dielectric background has not been subtracted.

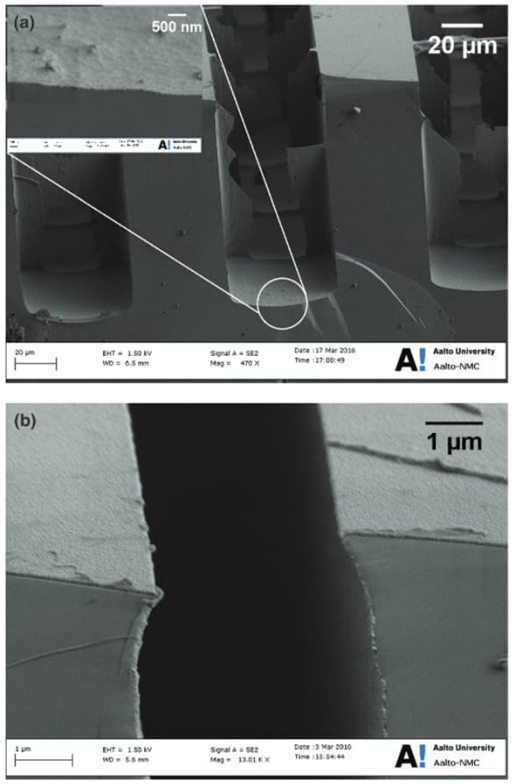

Fig. 10 SEM micrographs of trenches coated with $(Co_{1-x}Ni_x)_3O_4$ ($x = 0.33$): (a) typical trenches, the inset shows the film on the trench bottom, (b) film on top of a narrow trench.

4. Conclusions

High-quality ternary oxide $(Co_{1-x}Ni_x)_3O_4$ thin films spanning the whole composition range between Co_3O_4 and NiO were deposited by ALD for the first time. For films with Ni/(Co + Ni) ratios x ranging from 0 to 0.5, the dominant phase was of spinel type as proven by XRD while only for the higher Ni contents NiO was formed. This is an advantage compared to bulk materials for which the rock-salt structure is dominant for $x > 0.33$. Within the spinel-type region, electrical resistivity decreases with increasing Ni content. The resistivities of spinel films with Co contents of the stoichiometric composition $(Co_{2/3}Ni_{1/3})_3O_4$ (0.0014 Ω cm) and less (0.00107 Ω cm) were much lower than that of bulk $(Co_{2/3}Ni_{1/3})_3O_4$ and comparable to $(Co_{2/3}Ni_{1/3})_3O_4$ films prepared by PVD (0.003 Ω cm, Windisch *et al.*[20]) and laser-ablation epitaxy (0.00083 Ω cm, Bitla *et al.*[19]). These low resistivities increase the thermoelectric power factor of Co_3O_4 overcompensating the decrease of the Seebeck coefficient due to the doping.

D.J. Hagen, T.S. Tripathi, and M. Karppinen, Atomic Layer Deposition of Nickel-Cobalt Spinel Thin Films, Dalton Transactions, 2017, 46, 4796.

References

- Hofer, F., Schmidt, F.P., Grogger, W. & Kothleitner, G., (2016), Fundamentals of electron energy-loss spectroscopy, IOP Puplishing Ltd, Mat. Sci. Eng., **109**, 9 p., DOI: 10.1088/1757-899X/109/1/012007
- Egerton, R.F., (2009), Electron energy-loss spectroscopy in the TEM, IOP Puplishing Ltd, Rep. Prog. Phys., **72**, 25 p., DOI: 10.1088/0034-4885/72/1/016502
- Keast, V.J., (2012) Application of EELS in Material Science, Elsevier, Material characterization, **73**, 7 p., DOI: 10.1016/j.matchar.2012.07.013
- Gunay, H.B, Ghods, P., Isgor, B., Carpenter G.J.C. & Wu, X., (2013), Characterization of atomic structure of oxide films on carbon steel in simulated concrete pore solutions using EELS, Elsevier, Applied Surface Science, **274**, p. 195-202, DOI: 10.1016/j.apsusc.2013.03.014
- Laffont, L., Wu, M.Y., Chevallier, F., Poizot, P., Morcrette, M. & Tarascon, J.M., (2006), High resolution EELS of Cu–V oxides: Application to batteries materials, Elsevier, Micron, **37**, p. 459-464, DOI: 10.1016/j.micron.2005.11.007
- D.J. Hagen, T.S. Tripathi, and M. Karppinen, Atomic Layer Deposition of Nickel-Cobalt Spinel Thin Films, Dalton Transactions, 2017, 46, 4796.